



## Review on CFD analysis of horizontal falling film evaporators in multi-effect desalination plants

Furqan Tahir<sup>a</sup>, Abdelnasser Mabrouk<sup>a,b,\*</sup>, Muammer Koc<sup>a</sup>

<sup>a</sup>Division of Sustainable Development (DSD), College of Science and Engineering (CSE), Hamad Bin Khalifa University (HBKU), Education City, P.O. Box: 5825, Qatar, Tel. +974-44547453; emails: aaboukhlewa@hbku.edu.qa (A. Mabrouk), ftahir@mail.hbku.edu.qa (F. Tahir), mkoc@hbku.edu.qa (M. Koc)

<sup>b</sup>Qatar Environment & Energy Research Institute (QEERI), Research & Development Complex (RDC), Education City, P.O. Box: 5825, Qatar

Received 13 February 2019; Accepted 2 June 2019

---

### ABSTRACT

Desalination is a sustainable solution for water stressed countries. Among thermal desalination technologies, multi-effect desalination (MED) offers lower specific energy consumption. Falling film evaporators are extensively used in MED plants. This type of evaporator can achieve higher overall heat transfer coefficient and requires low liquid charge. The major challenges in these evaporators are (i) attaining uniform liquid load over tube bundle to avoid dry patches and scale formation, and (ii) achieving higher overall heat transfer coefficient. Although, experiments can characterize on a macroscopic scale, for microscopic understanding detailed numerical analyses is needed. This study focuses on critically analyzing the CFD works for MED falling film evaporator available in the literature. CFD modeling and methodologies have been presented followed by identification of key research gaps based on comprehensive discussion on hydrodynamics and heat/mass transfer aspects of falling film evaporators. The effects of thermophysical properties variation for broadening the operating range of MED plants, scale formation, CO<sub>2</sub> release, liquid load maldistribution outside tubes, uneven vapor flow inside vapor box and vapor flow in co-current/cross direction need more insight. Addressing these research gaps could assist in the development of optimum evaporator design with higher overall heat transfer coefficient, improved wettability and less susceptibility to scale formation can guarantee the evaporator performance.

*Keywords:* CFD; Falling film; MED; Evaporator; Desalination

---

### 1. Introduction

In order to overcome the growing need for fresh water, desalination is one of the promising and resilient solutions for countries adjacent to sea. Among desalination technologies, multi-effect desalination (MED) has gained an increasing attention in the past decade because of its lower specific energy consumption as compared with multi-stage flash (MSF) desalination, in addition, as a thermal desalination technology, it is more suitable for harsh seawater conditions as present in Gulf region. Furthermore, MSF technology has matured and reached its theoretical improvement

limits whereas MED still has room for further improvements potentially leading to further energy efficiency, emission reductions and productivity [1–3].

A typical MED plant consists of series of evaporators (effects) as shown in Fig. 1, which are usually of horizontal falling film type. These falling film exchangers have wide range of applications ranging from MED desalination, ocean thermal energy converters, Lithium bromide (LiBr)/ammonia-based air conditioning equipment (absorber and generator), petrochemical and food processing industries [4,5]. The advantages of falling film evaporators over flooded evaporators are their high heat transfer coefficient and low

---

\* Corresponding author.

liquid charge. These evaporators may achieve overall heat transfer coefficient up to 3,000 W/m<sup>2</sup>-K [6].

MED research has been focused to improve MED design for higher top brine temperature (TBT), lower scaling problem, reduced thermal losses and higher performance ratio. Mabrouk et al. [2,3] proposed integration of absorption vapor compression (AVC) instead of thermal vapor compression system to existing MED plants and modified evaporator design for uniform liquid load. Theoretical results have showed an increased performance ratio and reduced CAPEX and OPEX. In a design by Shahzad et al. [7], adsorption vapor compression (AdVC) was incorporated and distillate productivity was experimentally found to be doubled. Moreover, hybridization of desalination processes such as MED-RO, MED-MSF and RO-MSF have also been recommended in many studies [8–10] by enhancing productivity and reducing thermal losses and to minimize cost per unit distillate.

The main drawback of falling film evaporators in MED plants is the scale formation on tubes due to salts precipitation at high temperature and dry out regions. Due to salt precipitation problem, the TBT of MED plants is limited to 65°C and is preferred to the use of plain tubes. Tubes with enhanced heat transfer surfaces will be subjected to increased salt precipitation than the plain tubes due to more contact area and dry out regions. The lowest temperature, that is, in the last effect is restrained by ambient conditions [11,12]. The last effect temperature is mostly 42°C–45°C for Gulf Cooperation Council (GCC) region [13,14]. The number of effects in MED plants is dependent on TBT and last effect temperature difference. If this temperature difference is increased, it will thermodynamically allow more number of effects to be utilized, and hence, resulting in higher performance ratios.

Extensive experimental work has been carried out to characterize falling film hydrodynamics, flow pattern recognition, heat and mass transfer on plain and enhanced tubes [15–22]. Film distribution and flow patterns were found to be affected by different operating conditions such as liquid load and thermo-physical properties. Flow patterns were characterized into droplet, droplet-jet, jet (in-line and staggered), jet-sheet and sheet modes based on film Reynolds number and modified Galileo number [23,24] as shown in Fig. 2. The flow pattern mode and tube morphology have

significant effects on heat and mass transfer in falling film evaporators.

Although a significant number of experimental investigations have been carried out, falling film hydrodynamics is not fully understood yet. Improved evaporator design, increase in evaporator size, hybridization, improved tube materials and incorporation of AVC/AdVC will affect operating conditions, which may change falling film behavior. Therefore, it is important to characterize falling film for various operating conditions to identify optimal parameters for given goals and conditions. Computational fluid dynamics (CFD) is an effective tool to study fluid flow, heat and mass transfer on micro scale. In order to provide a comprehensive hydrodynamic understanding, this review focuses on numerical analyses and methods that have been carried out for horizontal falling film evaporator used in MED plants and other similar applications such as absorber, generator and evaporative condensers available in literature. The purpose of this study is to consolidate related numerical studies and methodologies in order to analyze and identify key research gaps. In addition, some experimental investigations have been discussed which are important in developing initial and boundary conditions for CFD case setup. Finally, an extensive and comparative discussion on CFD methodologies and recommendations are presented.

## 2. CFD approach

### 2.1. Mathematical modeling

There are three basic governing equations that describe flow dynamics and heat transfer of falling film; namely conservation of mass, momentum and energy.

$$\frac{\partial \rho}{\partial t} + \nabla \times (\rho \vec{V}) = S_m \tag{1}$$

$$\frac{\partial (\rho \vec{V})}{\partial t} + \nabla \times (\rho \vec{V} \vec{V}) = -\nabla P + \nabla \times (\bar{\tau}) + \rho \vec{g} + \vec{F} \tag{2}$$

$$\frac{\partial (\rho T)}{\partial t} + \nabla \times \left( \frac{k}{\rho C_p} \rho \vec{V} T \right) = \nabla \cdot (\nabla T) + S_e \tag{3}$$

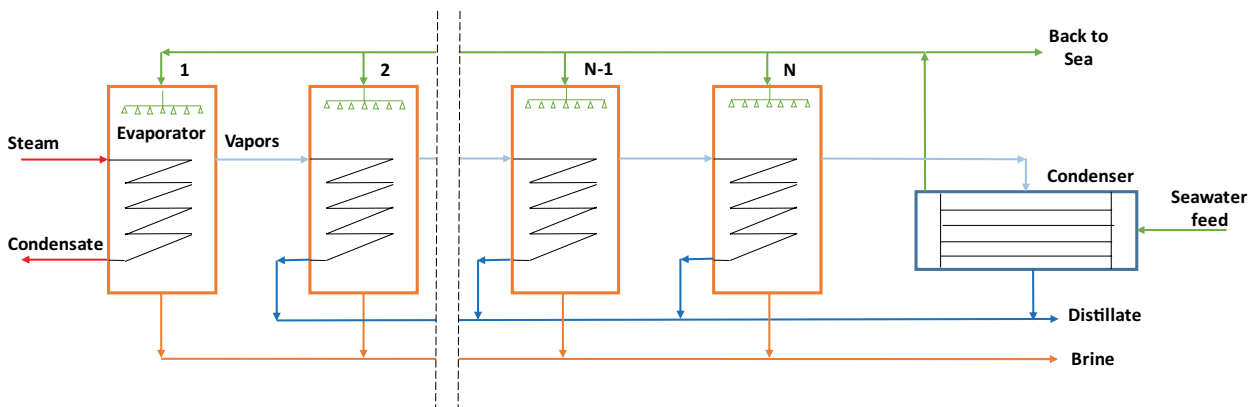


Fig. 1. Multi-effect desalination plant (MED) schematic.

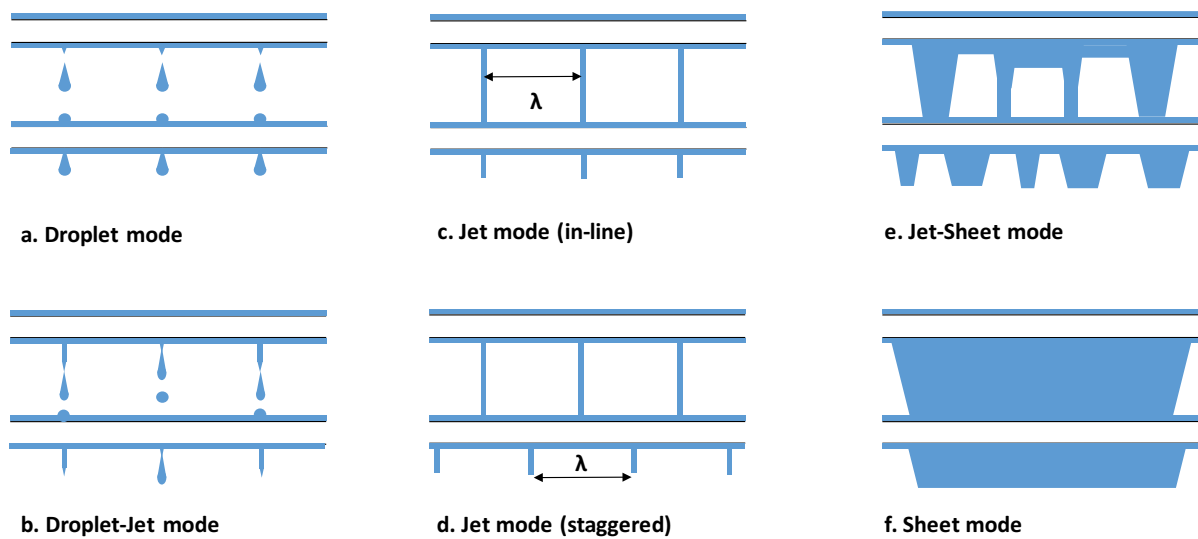


Fig. 2. Flow patterns in falling film horizontal tube.

where  $\rho$  is density,  $V$  is velocity,  $P$  is pressure,  $\tau$  is tensor,  $g$  is acceleration due to gravity,  $F$  is force,  $S$  is source term,  $T$  is temperature,  $k$  is thermal conductivity,  $C_p$  is specific heat and  $t$  is time.

Fig. 3 shows schematic of a single falling film horizontal tube evaporator used in MED desalination plants. Usually falling film evaporator is not studied numerically as a whole due to CFD model limitations, computational accuracy required, and computational power needed. Several regions within the evaporator require different CFD models. These CFD models cannot be coupled easily at the same time and are implemented separately for each region. In order to spread seawater feed uniformly over tube bundle and to avoid uneven distribution, solid cone nozzles are commonly used in industrial-scale evaporators [25–27]. These nozzles distribute feed into tiny droplets and spreading of droplets depends on solid cone angle  $\theta_c$  as shown in region 1 in Fig. 3. The number of nozzles is selected based on evaporator dimensions, solid cone angle, height from nozzle to first row and overlapping of sprays required as shown in region 2. For numerical investigations of droplets spreading and non-uniformity, dense discrete phase model is recommended but mostly in-house developed codes were developed by researchers to characterize spray hydrodynamics and save computational cost [28].

As the spray spreads over tubes, falling film is developed as shown in region 3. Falling film moves downward and heat is transferred from tubes to the film. Evaporation starts as the film temperature meets or exceeds saturation temperature. Vapors generated via evaporation gathers and moves towards demister. Vapor density is much lower than seawater density, so vapor flow may achieve higher velocities affecting falling film as shown in regions 4 and 5. Vapor flow direction may be either co-current or both co-current and cross flow.

### 2.1.1. VOF model

Falling film problem is complex in nature and with the increasing computational power; numerical modeling has

become feasible to analyze different flow modes dynamics. Capturing and tracking interface in multiphase flows efficiently is one of the key challenge. Hirt and Nichols [29] proposed volume of fluid (VOF) model based on Eulerian approach to locate and track free surface in multiphase flows. They modified conservation of mass for each phase using void fraction  $\alpha$ .

$$\frac{\partial(\alpha_i \rho_i)}{\partial t} + \nabla \times (\alpha_i \rho_i \vec{V}_i) = S_m \quad (i = g \text{ or } l) \quad (4)$$

where subscript  $g$  represents gaseous phase and  $l$  represents liquid phase.

Similarly, conservation of momentum and energy are solved for each phase as per Eqs. (2) and (3). The fluid properties such as density and viscosity  $\mu$  for each phase are computed based on volumetric average.

$$\rho = \alpha_l \rho_l + (1 - \alpha_l) \rho_g \quad (5)$$

$$\mu = \alpha_l \mu_l + (1 - \alpha_l) \mu_g \quad (6)$$

where:

$$\alpha_g = 1 - \alpha_l \quad (7)$$

Apart from falling film application [30–33], VOF model is widely used in multiphase flow problems such as capillary flows, bubble rise in quiescent liquid, Taylor bubble hydrodynamics, fluidization systems, reactors, flashing and open channel flows [34–37]. The accuracy of VOF model in capturing and tracking of liquid-gas interface is good but this model is transient and stability depends on Courant number. The Courant number is controlled by efficient meshing and lower time step, which make this model computationally expensive. The Courant number is discussed in detail in section 2.2.3.

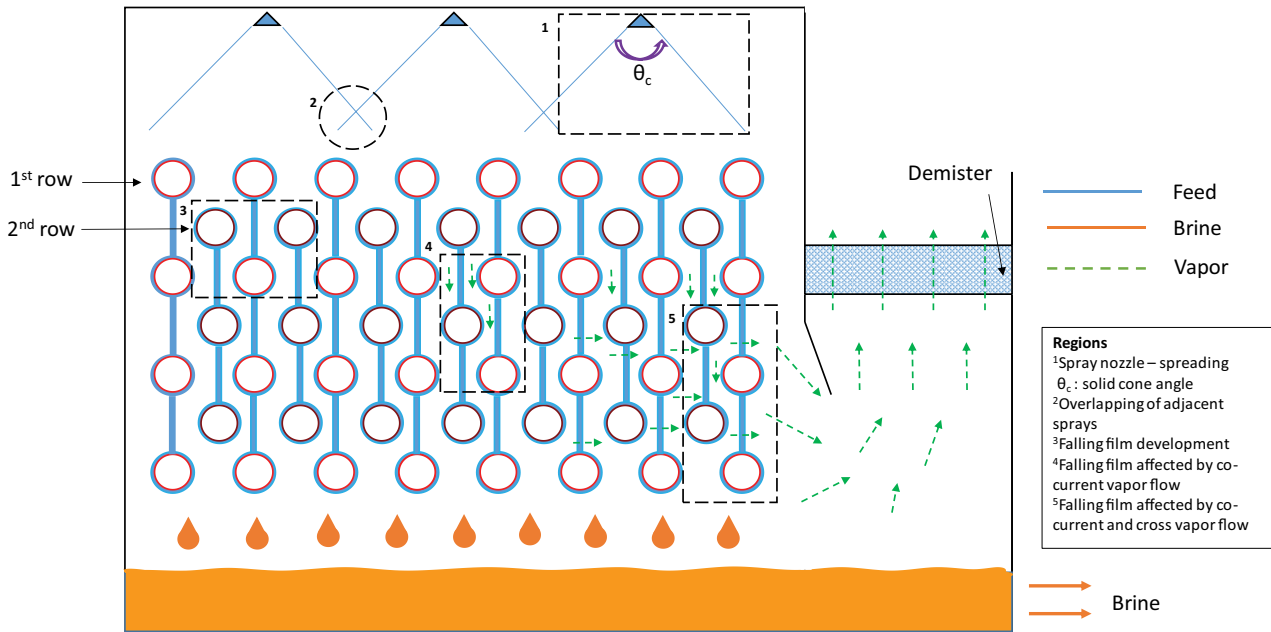


Fig. 3. Falling film horizontal tube evaporator for multi-effect desalination (MED) plant.

2.1.2. CSF model

Brackbill et al. [38] proposed continuum surface force (CSF) model to incorporate surface tension force. This model is used in falling film in conjunction with VOF model for better characterization of liquid gas phase interface. The volumetric surface tension force  $F_{vol}$  is added to momentum Eq. (2):

$$\bar{F}_{vol} = \sigma K \nabla \alpha_i \frac{\rho}{\frac{1}{2}(\rho_l + \rho_g)} \quad (8)$$

where  $K$  is the surface curvature and is evaluated from local gradients in the surface normal at liquid–gas interface.

$$K = -\nabla \times n \quad (9)$$

The surface unit normal vector  $n$  at cell next to wall for specified contact angle  $\theta_w$  is

$$n = n_w \cos \theta_w + t_w \sin \theta_w \quad (10)$$

where  $n_w$  and  $t_w$  are normal and tangential unit vectors, respectively. Although, CSF model gives results that are more accurate where surface tension effects are important, however this model requires additional term to solve in non-conservative and explicit manner. The continuum surface stress model can be used as an alternative.

2.1.3. Evaporation and condensation model

Lee [39] proposed a mechanistic model for evaporation and condensation, which can be coupled with VOF model

by source term as in Eq. (4). Based on this model, the mass source term will be as follows:

$$S_m = \beta_i \alpha_i \rho_i \left| \frac{T - T_{sat}}{T_{sat}} \right| \quad (11)$$

where  $T_{sat}$  is the saturation temperature,  $i = l$  for evaporation,  $i = g$  for condensation and  $\beta_i$  is the mass transfer time relaxation factor, which is usually 0.1 but can go up to 1,000 [40]. Large  $\beta_i$  values may induce numerical perturbation and instability and very small values may result in different interfacial temperature [41]. The required heat transfer for phase change can be evaluated by energy source term as:

$$S_e = S_m \times H_{lg} \quad (12)$$

where  $H_{lg}$  represents latent heat of vaporization or energy released/absorbed due to phase change phenomena.

2.2. CFD methodology

2.2.1. Correlations

In order to generalize experimental data, several correlations have been developed in the literature. These correlations can be used in conjunction with CFD modeling for comparison, developing boundary conditions and to save computational effort. Table 1 shows commonly used formulations for film thickness  $\delta$ , spacing between two neighboring jets  $\lambda$  and minimum film Reynolds number  $Re_{f,min}$ . Nusselt’s empirical relation [42] for film thickness is widely used in CFD work for comparison purpose [43–45]. As film thickness around the tube is usually less than 1 mm,

Table 1  
Falling film correlations for  $\delta$ ,  $\lambda$  and  $Re_{fmin}$

Parameters	Studies	Correlation	Remarks
Film thickness $\delta$	Nusselt [42]	$\delta(\theta) = \sqrt[3]{\frac{3\mu_l\Gamma_{1/2}}{\rho_l(\rho_l - \rho_g)g \sin\theta}}$	General correlation for $\delta$ . It was assumed that falling film flow pattern is in sheet mode
	Hou et al. [67]	$\delta(\theta) = C' \times \sqrt[3]{\frac{3\mu_l\Gamma_{1/2}}{\rho_l(\rho_l - \rho_g)g \sin\theta}} \left(\frac{s}{d}\right)^{n'}$	Incorporates effects of inter-tube distance $s$ and tube diameter $d$ . $C'$ and $n'$ are correction factors based on circumferential angle
	Mabrouk et al. [81]	$\frac{\delta_2}{\delta_1} = \sqrt[3]{\frac{\Phi}{d} - 1}$	Average film thickness on column based on 1st and 2nd rows differ as per this relation
Spacing between two neighbor droplets or jets $\lambda$	Yung et al. [83]	$\lambda = 2\pi \sqrt{\frac{n\sigma}{\rho g}}$	General correlation for $\lambda$ , strongly depends on surface tension and density of liquid phase
	Armbruster and Mitrovic [64]	$\lambda = \frac{2\pi\sqrt{2}}{\sqrt{\frac{\rho g}{\sigma} \left( 1 + \left( \frac{Re_f}{Ga^{\frac{1}{4}}} \right) 0.8 \right) + \frac{2}{d_0^2}}}$	Accounts effects of $Re_f$ and $Ga$ based on experimental data for isopropyl alcohol and water with $\pm 7.5\%$ uncertainty
Minimum Reynolds number $Re_{fmin}$ for wetting of bottom row	Lorenz and Yung [135]	$Re_{fmin} = 300$	Based on experiments, conducted on tube bundle with 30 rows. $Re_{fmin}$ was introduced as fixed number and independent of thermophysical properties, heat flux and bundle configuration
	Fujita and Tsutsui [17]	$Re_{fmin} = \frac{q}{48}$	Based on refrigerant R-11 experimental data conducted on five tubes under constant heat flux condition
	Roques and Thome [18]	$Re_{fmin} = 164 + 6.8 \frac{q}{1000}$	Based on refrigerant R-134a experimental data under constant heat flux condition

for which fine grid is required to capture hydrodynamics of falling film with accuracy; this makes VOF model quite computationally expensive. This is the reason that a section of tube(s) is considered for numerical domain. From  $\lambda$  correlations in Table 1, tube section length can be computed for droplet and jet modes and only section equivalent to this length will be enough to generalize flow around the tube using symmetric boundary conditions. From  $Re_{fmin}$  empirical relations, liquid load and heat flux may be computed and used to investigate other parameters. Table 2 includes the empirical relations developed for transitional film Reynolds number as a function of modified Galileo number  $Ga$ . These relations differ slightly from each other as these were developed using different experimental data and operating conditions. The dissimilarities in transitions are quite evident in Fig. 4. Apart from the transitions overlapping, there is a wide range where flow pattern is fixed, from which liquid load can be computed to investigate certain mode as required.

### 2.2.2. Meshing

Mesh size, quality and type of elements are key factors that affect rate of convergence, accuracy and computational time. Structured elements (hexahedral in 3D and

quadrilateral in 2D) have good precision, better process adaptability and robust boundary recognition ability as compared with unstructured grid (tetrahedral/pyramid in 3D and trigonal in 2D). In addition, coarser elements, high skewness and aspect ratios can lead to unwanted errors [46]. Mesh type, no of elements, elements per unit area/volume for VOF model studies are listed in Tables 3 and 4. It is evident from these tables that relative coarser grid was used in some literature [33,47–49] and fine grid was used in some studies [31,32,44,50–55]. Most of the studies implemented quad/hexahedral elements except [33,56], they used trigonal elements instead.

Based on numerical studies and CFD best practices, quad-pave/quad o-grid for 2D and hexahedral with o-grid for 3D are recommended elements for VOF model. Most of the researchers have chosen minimum element size in the range of 0.01–0.02 mm near tube wall to capture film distribution accurately around the tube. If the whole domain is meshed with fine elements, it will be computationally expensive. However, region where gradients are expected to be high or where liquid phase (in case of no vapor flow) may exist can be meshed with fine elements and coarser elements can be used for rest of the domain. This can be accomplished by either incorporating boundary layers as shown in Fig. 5 or employing mesh adaption techniques [57–59].

Table 2  
Summary of correlations for flow mode transitions available in literature

Studies	Transition			
	Droplet to droplet-jet	Droplet-jet to jet	Jet to jet-sheet	Jet-sheet to sheet
Hu and Jacobi [23,132,133]	$Re_f = 0.074Ga^{0.302}$	$Re_f = 0.096Ga^{0.301}$	$Re_f = 1.414Ga^{0.233}$	$Re_f = 1.448Ga^{0.236}$
Roques et al. [24]	$Re_f = 0.0417Ga^{0.3278}$	$Re_f = 0.0683Ga^{0.3204}$	$Re_f = 0.8553Ga^{0.2483}$	$Re_f = 1.068Ga^{0.2563}$
Roques and Thome [134]				
Mitrovic [22]	$Re_f = 0.34Ga^{0.25}$	$Re_f = 0.34Ga^{0.25}$	$Re_f = 0.92Ga^{0.25}$	$Re_f = 1.08Ga^{0.25}$
Armbruster and Mitrovic [64]	$Re_f = 0.2Ga^{0.25}$	$Re_f = 0.26Ga^{0.25}$	$Re_f = 0.94Ga^{0.25}$	$Re_f = 1.14Ga^{0.25}$

Where:  $Ga = \frac{\rho\sigma^3}{\mu^4g}$

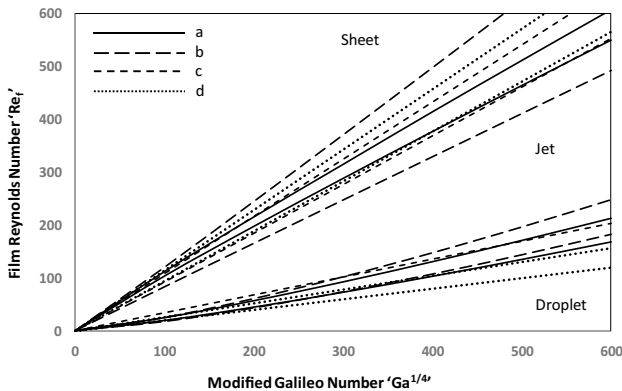


Fig. 4. Flow pattern transitions based on experimental data (a) Hu and Jacobi [23,132,133], (b) Roques et al. [24], Roques and Thome [134], (c) Mitrovic [22], and (d) Armbruster and Mitrovic [64].

Hosseinnia et al. [43] used adaptive mesh technique known as *h*-refinement. In this refinement, region that is subjected to dynamic volume fraction gradient is divided into finer elements.

2.2.3. Solver settings and time step independence check

Based on the CFD studies, solver settings are summarized in Table 5. Mesh and time step independency are crucial for computational accuracy and time. These independency checks are made to ensure trade-off between accuracy and power required and these checks should be made available in the study for re-production and comparison purposes. Many studies as shown in Tables 3 and 4 did not provide mesh and time step details. Furthermore, studies that mentioned time step size, it varied from 0.03 [48] to 1 ms [60], which is a wide range. Such time step size, mesh size per unit area/volume variation and incomplete data may reflect discrepancies in the results.

Table 3  
Mesh and time step details of VOF studies for 2D

#	Studies	Mesh type	Elements (Minimum size)	Elements per unit volume/area	Time step (ms)
1.	Qiu et al. [32,52]	Quad	70 k (0.01 mm)	87 <sup>a</sup>	0.10
2.	Abraham and Mani [60,106]	Quad – Pave	10 k	–	1
3.	Yang et al. [51]	Quad	52 k	89.8 <sup>a</sup>	0.05
4.	Hassan et al. [70]	Quad	– (0.4mm)	–	Variable
5.	Sun et al. [49]	Quad	8.6 k	5.9 <sup>a</sup>	1
6.	Zhao et al. [45,90]	Quad	7.63 k (0.1 mm)	–	0.005–0.050 (Co < 0.15)
7.	Lin et al. [115]	Quad – O grid	9.12 k (0.1 mm)	–	–
8.	Luo et al. [112]	Quad	10.6 k	–	–
9.	Fiorentino and Starace [33]	Triangular – pave with quad boundary layer	24.5 k (0.15 mm)	5.4	–
10.	Ji et al. [56]	Triangular	75.93 k	33	–

<sup>a</sup>Approximated due to unavailability of data.

Table 4  
Mesh and time step details of VOF studies for 3D

#	Studies	Mesh type	Elements (minimum size)	Elements per unit volume/area	Time step (ms)
1.	Ding et al. [44]	Hexahedral – O-grid	1.8 M ( $0.2 \times 0.2 \times 0.02 \text{ mm}^3$ )	101	0.05
2.	Fernandez de Arroioble et al. [72,73]	Hexahedral	1.04 M (0.06 mm)	–	–
3.	Li et al. [48]	Hexahedral	1.4 M (0.075 mm and 2.22 mm)	3.93	0.03
4.	Chen at al. [62]	Hexahedral	–	–	–
5.	Hosseinnia et al. [43]	Hexahedral with adaptive mesh refinement	– ( $0.2 \times 0.2 \times 0.0125 \text{ mm}^3$ )	–	–
6.	Qiu et al. [31] Zhang et al. [65]	Hexahedral – O-grid	780 k (0.02 mm)	171 <sup>a</sup>	<0.05
7.	Killion and Garimella [53] Subramaniam and Garimella [54,55]	Hexahedral	1.19 M (0.1 mm)	474 <sup>a</sup>	0.20
8.	Qi et al. [50]	Hexahedral	1.42 M (0.1 mm)	263.8 <sup>a</sup>	–
9.	Qiu et al. [66]	Hexahedral – O-grid	780 k (0.02 mm)	–	0.10
10.	Zhou et al. [47]	Hexahedral	10.21 k	22.7	–

<sup>a</sup>Approximated due to unavailability of data.

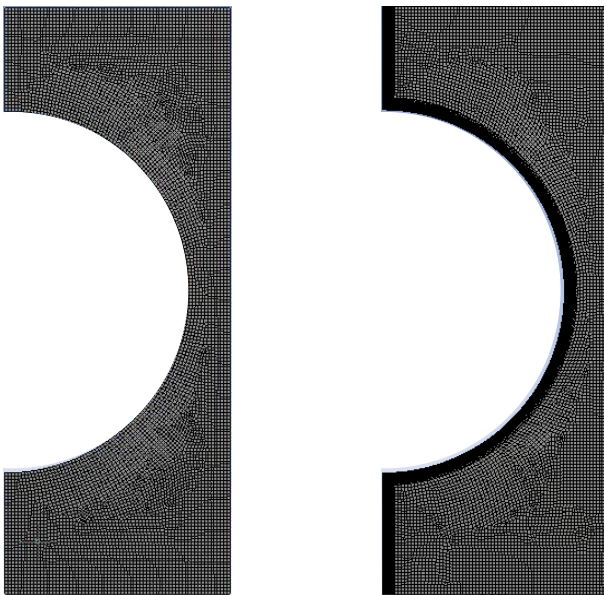


Fig. 5. (a) Quad mesh and (b) quad mesh with boundary layers.

For the VOF model, Courant number  $Co$  should be kept low  $\leq 0.25$  as a stability criterion, for 3D it is defined as follows:

$$Co = \frac{u\Delta t}{\Delta x} + \frac{v\Delta t}{\Delta y} + \frac{w\Delta t}{\Delta z} \quad (13)$$

where  $u$ ,  $v$  and  $w$  are respective velocities in  $x$ ,  $y$  and  $z$  directions.

It is clear from above equation that by adopting good mesh and lower time step, Courant number can be controlled. For large inter-tube spacing where free falling velocity may be high or larger liquid load, time step can be made variable to control required Courant number.

### 3. Hydrodynamic characteristics

CFD studies based on VOF methods for falling film hydrodynamics are listed in Table 6.

Table 5  
Recommended solver settings for VOF model

Settings	Recommendation
Flow regime	Laminar or turbulent (as per [136])
Surface tension modeling	CSF model
Volume fraction cut-off	$10^{-6}$
Courant number	$\leq 0.25$ ( $\leq 1.0$ [48])
Transient formulation	1st order implicit
Pressure velocity coupling	PISO/SIMPLE algorithm
Pressure interpolation scheme	PRESTO algorithm
Discretization	2nd order upwind (momentum and energy)
Surface tracking/volume fraction	Geo reconstruct
Evaporation model	Lee model [39]

Table 6  
CFD studies for falling film hydrodynamics using VOF method

Studies	Domain	Working fluid	Assumptions	Flow mode	Parameters varied	Parameters observed	Key findings
Ding et al. [44]	3 tubes, $s = 25.4$ mm, $d = 12.7$ mm, $L = 22$ mm	Water + air	TPP at 20°C, $q = 0$	D, J	$\theta_w = 30^\circ$ & $60^\circ$ $\Gamma_{1/2} = 0.02$ & $0.05$	Flow dynamics, wettability	Wetted area decreases and liquid elongation distance in axial direction decreases as the contact angle increases
Fernandez de Arroyable et al. [72,73]	One and half tube $s = 12.25$ mm, $d = 19.05$ mm	LiBr sol + water vapor	Constant TPP, $q = 0$	D, D-J, J	$\theta_w = 0^\circ - 120^\circ$ , $Re_j = 7, 24, 53$	WR	For each $\theta_w$ there is a minimum value of $Re_j$ at and above which tube wetting is 100%
Li et al. [48]	2 tubes, $d = 16$ mm, $s = 15$ mm, $L = 100$ mm	Water + air	$\theta_w = 0^\circ$ , TPP at 20°C $q = 0$	D, J, S	$\Gamma_{1/2}$ $V_s = 0 - 0.5375$ m/s	Flow pattern transition $Re_j$	$\delta$ increases as counter current vapor velocity increases
Qiu et al. [32,52]	2 tubes, $d = 19.05$ mm, $s = 6.4$ mm	Water + air	$\theta_w = 0^\circ$ , TPP at 20°C $q = 0$	-	$Re_j = 480-880$ , $d = 19-90$ mm, $s = 6-19$ mm	$\delta$	$\delta$ increases as $Re_j$ increases or inter-tube spacing $s$ increases. $\delta$ decreases as $d$ increases but the effect is minimum
Chen et al. [62]	3 tubes (staggered) $O = 2 \times 2$ mm <sup>2</sup> , $d = 14$ mm, $s = 14$ mm	Water-air	TPP at 20°C, $q = 0$	D, D-J, J, J-S, S	$mi = 0.0003-0.02$ kg/s	Flow pattern transitions	Critical flow rate for droplet to columnar was found to be 0.0125 kg/s
Qiu et al. [31]	1 tube	Water + air	Constant TPP, $q = 0$ , $\theta_w = 0^\circ$	J (In-line & staggered)	$v = 0.6$ m/s	Flow mode, $\delta$	Critical flow rate for columnar to sheet was found to be 0.02 kg/s
Zhang et al. [65]	$d = 25.4$ mm, $L = 11$ mm	Water + air and ethylene glycol + air	Constant TPP at 27°C, $q = 0$ , $\theta_w = 0^\circ$ , $V = 0.52$ m/s.	-	$v = 10, 20$ & $30$ mm	$\delta$	Formation of in-line and staggered mode is related to Plateau-Rayleigh instability
Hassan et al. [70]	2 tubes $d = 19.05$ mm, $s = 10$ mm, $wd = 20$ mm	Water + air	Constant TPP at 25°C, $q = 0$ , laminar	D	Initial $\delta = 0.20-0.50$ mm	Droplet formation	Lower $\delta_{avg}$ for increased inter-tube spacing
Killion and Garimella [53]	1 tube $d = s = 15.9$ mm	LiBr sol (55%wt) + air	Constant TPP at 25°C, $q = 0$ , laminar	-	-	-	3D model was found to be more accurate and was recommended to study hydrodynamics of falling films
Sun et al. [49]	1 tube and 2 tube $d = 50$ mm, $O = 2.5$ mm, $h_i = 12.5$ mm	Water + air	Constant TPP, $q = 0$ , Laminar	-	$h_i = 12.5, 25$ and $50$ mm, $v = 0.3-1$ m/s	$\delta$	Increasing $\Gamma_{1/2}$ reduces $\delta$ variation over time. $\delta$ reduces as $h_i$ increases

Zhao et al. [45]	1 tube $O = 2$ mm, $d = 25.4$ mm, $h_i = 6.3$ mm	Water + air	$q = 0$ , $\theta_w = 10^\circ$ , Laminar	-	$\Gamma_{1/2} = 0.025$ – 0.284 kg/m-s, $h_i = 3$ –50.8 mm, $d = 6.35$ –50.8 mm, $T = 2^\circ\text{C}$ –104°C	$\delta$	$\sigma$ affects $\delta$ distribution and recirculation within the film, but effects become minimal with an increase of $\Gamma_{1/2}$ . New correlation of $\delta$ was proposed $\delta_{\max}$ at crest is more than three times of $\delta_{\min}$
Qiu et al. [66]	1 tube $d = 25.4$ mm, $O = 2$ mm, $L = 11$ mm	Water + air	Constant TPP, Laminar, $q = 0$	J	$Re_j = 171$ –368	$\delta$	
Fiorentino and Starace [33]	2 tubes (staggered) $d = 25$ mm, $\phi_y = 50$ mm, $\phi_x = 100$ mm	Water + moist air	Counter current airflow, Constant $T_w$ Turbulent	D, J	$\dot{m}_{\text{air}} = 0.16$ & $0.25$ kg/s, $\dot{m}_{\text{water}} = 0.25$ , $0.33$ , $0.44$ & $0.55$ kg/s	Film stability and detachment	An increase of 73% in $\phi_y$ requires 66.7% more $\dot{m}_{\text{water}}$ for film stability and to avoid film break up
Ji et al. [56]	one tube, $d = 16$ mm, orifice = 1 mm, $h_i = 5$ mm	LiBr sol + water vapor	Constant TPP, $q = 0$ , laminar	-	$\theta_w = 0^\circ$ –80°, $\Gamma_{1/2} = 0.0683$ – 0.429 kg/m-s	Wettability and $\delta$	$\delta_{\min}$ occurs at 120°, based on this Nusselt correlation was modified. Higher $\theta_w$ and lower $Re_j$ leads to reduced wettability

D = droplet, J = Jet and S = sheet.

### 3.1. Wettability effect

#### 3.1.1. Flow modes

Based on developed empirical relations in Table 2, transitions from one flow mode to another depends on film Reynolds number and modified Galileo number. These correlations do not account for tube morphology/wall adhesion, as most of the experiments were performed with surface treated tubes with lower contact angle and excluded the effects of vapor flow, which may affect transitional film Reynolds number. For flow mode recognition and quantification, high speed image processing is commonly used. Most of the experimental work are focused on macroscopic phenomena, however in order to fully understand the transitional behavior at the microscopic level due to complexity of the falling film, numerical studies were implemented.

Generally droplet and jet modes are investigated as most of the commercial units such as absorber, generator and evaporators are designed based on droplet and jet modes [43,44,61]. Killion and Garimella [53] were amongst the first to study droplet formation in horizontal tubes using VOF model in 3D domain. They used initial film thickness with periodic boundary conditions instead of liquid load via orifice, which is nowadays, has become usual practice. The shape of droplet formation, falling, merging, spreading and detachment were compared experimentally and numerically and found to be in good agreement. Results showed that impact time decreases from 611 to 98 ms when initial film thickness in increased from 0.23 to 0.40 mm, which is due to the higher liquid load and velocity field.

Qiu et al. [31] investigated formation and hydrodynamic characteristics of in-line and staggered jet modes using two sets of fluids, that is, water–air and ethylene glycol–air. Their CFD model was validated qualitatively with the experimental data. They found that formation of in-line and staggered mode is related to Plateau-Rayleigh instability. As the fluid impacts on tube, it moves downward and in axial direction due to which propagation waves underside of tube may generate excess liquid at either beneath the upstream jet (in-line mode) or in between two upstream jets (staggered mode). This excess liquid from departure site detaches and form downstream jet. In-line jet mode was developed in ethylene glycol case, where two adjacent jets impact and spread over tube surface. Fig. 6a shows formation of trough in between two adjacent jets as liquid spreads and then jets are formed under the tube in same line (in-line) before the whole tube is fully covered. The film continues to spread axially causing whole tube to cover with liquid film. However, staggered jet mode was formed in water case where two adjacent jet impacts and a crest is formed (Fig. 6b) in between two adjacent jets and jet under the tube is not formed until whole tube is covered with liquid film. In addition, viscous force plays vital role in developing in-line or staggered jet mode.

Chen et al. [62] experimentally and numerically found critical mass flow rate for flow pattern transition using three 14 mm diameter tubes in triangular configuration. Critical mass flow rate for droplet to columnar was found to be 0.0125 kg/s from simulations and 0.013 kg/s from experimental data. Critical flow rate for columnar to sheet was found to be 0.02 kg/s from simulations and 0.0215 kg/s from experiments. The difference in both methodologies may

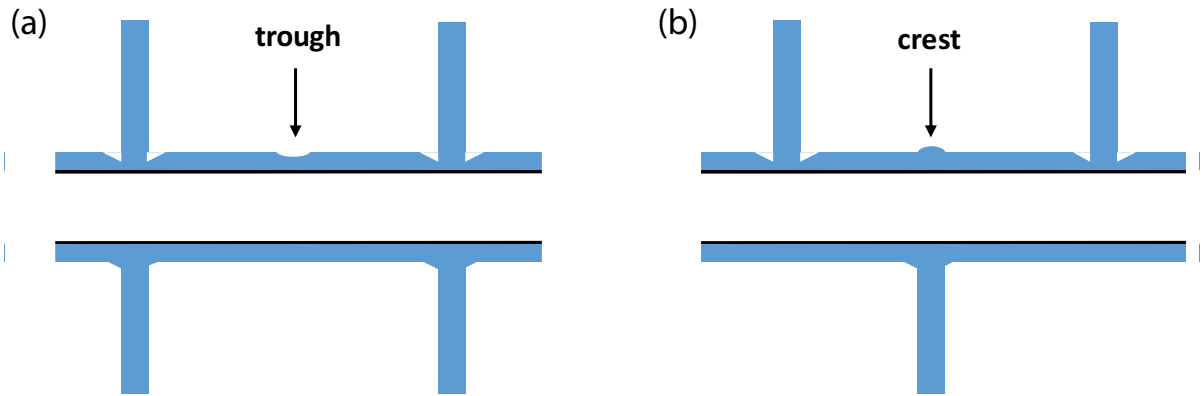


Fig. 6. (a) Trough formation in in-line jet mode and (b) crest formation in staggered jet mode.

come from uncertainties in experimental setup and simplified assumptions in CFD setup. However, modeling details such as mesh details, time step, mesh and time independency checks were not provided. Recently Ding et al. [44] studied hydrodynamics of droplet and jet modes in falling film horizontal tubes using commercial CFD software Ansys fluent. In their study, first they validated their model by flow comparison with experimental data available in the study by Killion and Garimella [63] and film thickness with Nusselt correlations [42]. Then they analyzed the effect of contact angle, liquid load and initial conditions on droplet formation, droplet detachment, droplet impact, flow stability, formation and wettability. They considered three tubes of 12.7 mm diameter with 22 mm section length calculated by Armbruster and Mitrovic [64] correlation as shown in Table 2. It was found that when a droplet influences the tube surface in a droplet mode, circumferential film thickness raises and then decreases as the droplet leaves for the next tube. So, in a droplet mode, film around the tube changes as droplet impacts and leaves; making this process unsteady and cyclic. Whereas, falling film in a jet mode may achieve steady state with weak perturbations. Although, numerical studies helped in understanding flow mode transition but still more insight is needed to address the effect of thermophysical properties variations such as salinity, viscosity, surface tension and addition of chemical agents from one effect to another, for MED evaporators.

### 3.1.2. Falling film formation and force analysis

Fig. 7 shows different type of forces acting on falling film with an assumption of insignificant vapor flow (shear force may be neglected). These forces exert on film due to gravitation, adhesion, viscous effects and surface tension. From numerical studies, falling film formation can be summarized into following stages [32,44,45,65,66].

- Free falling of film: Through the orifice or before tube liquid phase moves in y direction under the action of gravity and surface tension force as shown in Fig. 8a. If liquid load is small, the surface tension force will be substantial to oppose gravitational force causing the liquid phase to form droplets and flow mode will be droplet. For higher liquid load, gravitational force is

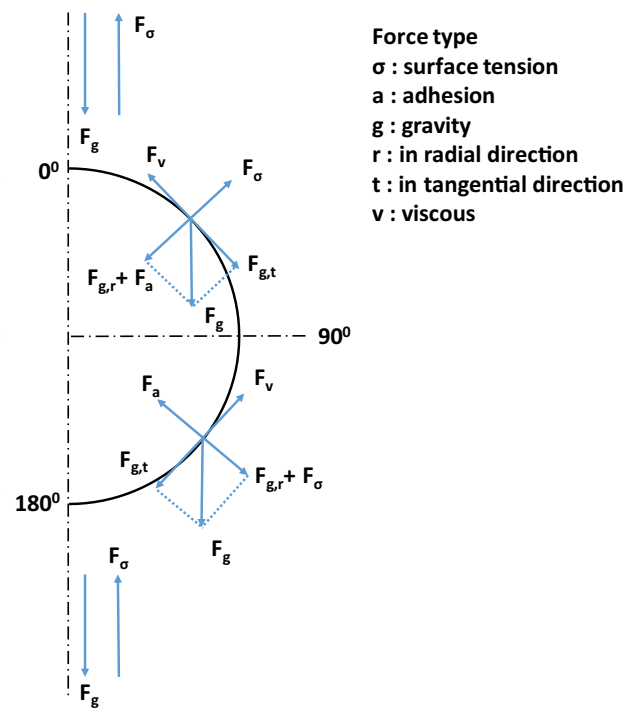


Fig. 7. Type of forces acting on falling film at different stages.

much greater than surface tension force, which raises y-velocity hence producing jet mode.

- Falling film stagnation and impact/impingement zone: As free falling film strikes tube surface at  $\theta = 0^\circ$ , y-velocity becomes zero and there is a sudden pressure loss and turbulence in the film. Film then spreads over tube surface in axial and downward direction as shown in Fig. 8b. Because of the turbulence and high velocity gradients, heat transfer coefficient is expected to be high in this region.
- Developing region: In this region, falling film moves under tangential gravitational force opposes by viscous drag force as shown in Fig. 8c. The velocity profile within the falling film develops and laminar sub-layer thickness decreases with angular position. Laminar sub-layer thickness decreases film heat transfer resistance and

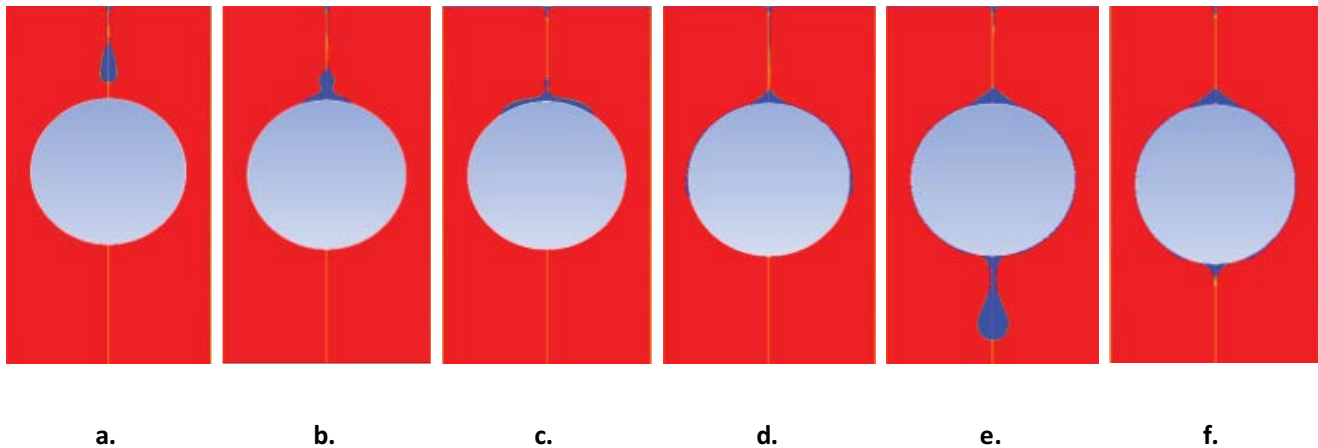


Fig. 8. Falling film formation (a) free fall, (b) stagnation point and impingement zone, (c) developing region, (d) developed region, (e) film detachment and (f) necking.

increases heat transfer due to the presence of laminar and turbulent regions. For small tube diameter and higher liquid load, developing region is expected to be high which means higher average heat transfer coefficient.

- Developed region: In this region, velocity profile is fully developed and liquid film covers most of the tube surface as shown in Fig. 8d, which results in higher conduction resistance. In the lower part of the tube, surface tension force is accompanied by gravitational force component in the radial direction. However, in the upper part, surface tension is opposed by radial gravitational force. This is the reason that results in asymmetric film distribution in the upper and lower half of tube.
- Detachment region: Liquid film moves downward from both sides and meet at the lowest position of tube ( $\theta = 180^\circ$ ). As more liquid film is added, it detaches from the tube surface and now there are only surface tension and gravitational force as shown in Fig. 8e. For lower liquid load, surface tension force gathers liquid as much as possible and shape of liquid becomes more spherical (droplet). When liquid gathers enough to counter surface tension, it detaches and falls freely over next tube.
- Necking: As droplets detach, the thickness of remaining film decreases as shown in Fig. 8f. Surface tension force becomes high and lift the remaining liquid upwards momentarily and again more liquid gathers and form droplet shape. For jet and sheet modes, falling film is continuous but the thickness reduces due to higher liquid load which overcomes surface tension effects making flow steady state with some weak perturbations.

### 3.1.3. Falling film thickness

Falling film thickness  $\delta$  was measured experimentally in many studies but the limitations exist, such as number of locations covered and readings of certain location may be affected by upstream sensor. Roger and Goindi [16] measured film thickness with an uncertainty of  $\pm 5\%$  at three different locations  $\theta = 45^\circ, 90^\circ$  and  $135^\circ$  using dial gages connected with an electrical circuit. Hou et al. [67] measured film thickness for  $\theta = 15^\circ$ – $165^\circ$  using a displacement micrometer.

Gstoehl et al. [68] used laser technique to examine film thickness with an uncertainty of  $\pm 7\%$ ; but due to visualization restraints, they could only measure for  $\theta = 22^\circ$ – $62^\circ$  and  $\theta = 112^\circ$ – $152^\circ$ . However, their technique avoided distribution in the film. These experimental studies are widely used for CFD model validation.

There are many inconsistencies for film thickness pattern, like it was observed experimentally and numerically that the minimum film thickness in a jet mode is half of the maximum film thickness [44,48,69]; while in another study maximum film thickness was found to be more than three times of minimum film thickness for jet mode [66]. In another study [60], film detachment, film disintegration, splashing was reported for an array at higher Reynolds number ( $Re_f = 1,250$ ) but no such phenomena was reported in other studies at higher  $Re_f$  [45,49,51]. Furthermore, minimum thickness  $\delta_{\min}$  location from numerical studies varies from  $\theta = 90^\circ$ – $140^\circ$  for different operating conditions as shown in Table 7. However, consensus was made for asymmetric film profile in the upper and lower half of tube as compared with symmetric profile as inertial forces were neglected in Nusselt correlation [45,49].

Hassan et al. [70] studied inter-tube spacing effects on film thickness. In their study, it was observed that increasing inter-tube spacing results in reduced film thickness due to added momentum and higher velocity field within the film. They compared their results with Hou et al. [67] correlation for film thickness and found within  $+50\%$ . Another study by Sun et al. [49] supports above finding that an increase in inter-tube spacing decrease film thickness. These findings align with film thickness correlation developed by Hou et al. [67] in which inter-tube spacing effects are incorporated. However, according to Zhang et al. [65] inter-tube spacing has minimal effect on film thickness.

Qiu et al. [32,52] studied effect of films Reynolds number/liquid load under adiabatic conditions. They considered two horizontal tubes with  $d = 19.05$  mm in a 2-D domain. CFD model was compared with Nusselt correlation and error was found within  $20\%$ . It was observed that increasing  $Re_f$  from 480 to 880 leads to liquid film detachment near bottom stagnation point causing an early departure. The inter-tube

Table 7  
Angular position for  $\delta_{\min}$

Studies	$\theta$ for $\delta_{\min}$	Remarks
Qiu et al. [31]	90°	In-line jet mode
	120°	Staggered jet mode
Wang et al. [137]	90°	$\Gamma_{1/2} = 0.4$ kg/m-s
Qiu et al. [52]	90°–140°	$Re_f = 480$ –880
Li et al. [48]	90°–100°	Without vapor flow
	70°–80°	Counter current vapor flow
Sun et al. [49]	120°–130°	$v = 0.05$ –1 m/s
Zhao et al. [45]	110°–150°	$\Gamma_{1/2} = 0.103$ –0.284 kg/m-s
Lou et al. [112]	125°	Circular tube
	160°	Oval shaped tube
	170°	Drop shaped tube
Zhou et al. [47]	100°–140°	Coupled heat transfer
Ji et al. [56]	120°	Wall adhesion effects
Hou et al. [67]	90°–115°	Experimental study

spacing was also varied from  $s = 6$  to 19 mm and film thickness was reduced by 15% due to added momentum, which causes rapid liquid spreading over tube. In addition, the effect of diameter was observed, and it was deduced that increment in diameter leads to reduced film thickness. This happens because more curvature effect assists gravitational force and rise in tangential force results in increased velocity field, but the effect is minimum for diameter  $d > 32$  mm. Qiu et al. [31,66] concluded that regions where film thickness is low, spreading velocity is high as compared with other regions; so spreading velocity and film thickness have inverse relation. In addition, in the axial direction of in-line jet mode, maximum film thickness was found at jet and minimum film thickness was found in between two adjacent jets/at the center of trough. For staggered jet mode, maximum film thickness was found in between two adjacent jets/at the center of crest and minimum film thickness was located at upstream jet.

Nusselt correlation is commonly used but it assumes symmetric profile. Hou et al. [67] modified Nusselt correlation and incorporated asymmetric, inter-tube spacing and diameter effects with the help of experimental data. There are also some correlations that were developed using numerical data. In one study, Ji et al. [56] found minimum thickness at  $\theta = 120^\circ$  for different operating conditions. So, they modified Nusselt correlation [42] and shifted minimum thickness to  $120^\circ$  as per below:

$$\delta(\theta) = \sqrt[3]{\frac{3\mu_l\Gamma_{1/2}}{\rho_l(\rho_l - \rho_g)g\sin\left(\frac{3\theta}{4}\right)}} \quad (14)$$

Lately, Zhao et al. [45] numerically studied falling film for various liquid load  $\Gamma_{1/2}$ , viscosity  $\mu$ , tube diameter  $d$ , surface tension  $\sigma$  and impingement height  $h_i$ . They found that each parameter affects falling film to some extent and presented

a new correlation incorporating all these factors, which is as follows:

$$\frac{\delta}{d} = C_a Re_f^{a_1} We^{a_2} Ar^{a_3} \left(\frac{h_i}{d}\right)^{a_4} \left(\frac{\pi\theta}{180}\right)^{a_5} \quad (15)$$

where films Reynolds number  $Re_f = 400 - 2,485$ , modified Weber number  $We = 4.55 \times 10^{-4} - 21.4 \times 10^{-4}$ , Archimedes number  $Ar = 7.17 \times 10^6 - 3.67 \times 10^9$ , impingement height to diameter ratio  $h_i/d = 0.12 - 2$ ,  $C_a, a_1, a_2, a_3, a_4$  and  $a_5$  are constants, which are evaluated for  $\theta = 2^\circ - 15^\circ, 15^\circ - 165^\circ$  and  $165^\circ - 178^\circ$  using regression analysis. They tested above correlation for presented and available data in the literature and found most data fit within  $\pm 20\%$  error for  $\theta = 2^\circ - 165^\circ$  and within  $\pm 30\%$  error for  $165^\circ - 178^\circ$ .

However, above correlation accounts for surface tension effects but in development process, numerical cases were set with and without surface tension. The variation of surface tension with temperature was not incorporated. The location of minimum film thickness is not fixed at  $90^\circ$  as per Nusselt solution and depends on several factors, Table 7 shows minimum film thickness variation for different operating conditions and configuration. The minimum film thickness location needs more insight as it may define the limitation of liquid load in MED evaporators and susceptibility to scale deposition.

### 3.1.4. Effect of wall adhesion

In most of the CFD studies [31,32,48,52,65], wall adhesion effects are neglected, and it was assumed that the tubes are completely wet (contact angle  $\theta_w = 0^\circ$ /super hydrophilic) for simplicity. For super hydrophilic materials, tubes may achieve 100% wettability for very low flow rates but as the contact angle increases, wettability depends on flow rate and initial conditions. However, for materials commonly used for evaporator tubes in MED plants, static contact angle varies from  $60^\circ$  to  $90^\circ$  [71]. There are limited numbers of CFD studies, which addresses the effect of wall contact angle on wettability. Zheng et al. [21] conducted experiments on super hydrophilic ( $\theta_w < 5^\circ$ ), hydrophilic ( $\theta_w = 27.8^\circ$ ) and plain copper ( $\theta_w = 43.7^\circ$ ) horizontal tubes under heat transfer and low liquid load conditions. Super hydrophilic tubes were established by using strong oxidant. It was observed that heat transfer coefficient for super hydrophilic tubes was higher than that of plain tubes for the same Reynolds number. This was due to the fact that at even low liquid load, liquid spreads over tubes rapidly and there were no dry patches, which caused lower thermal resistance and high heat transfer coefficient was measured for super hydrophilic tubes. At lower liquid load, super hydrophilic and hydrophilic were found completely wet while plain tubes had some dry patches. However, controlling contact angle is difficult and costly for experiments.

Fernandez de Arriola et al. [72,73] conducted CFD simulations for various contact angles  $\theta_w = 0^\circ - 120^\circ$  with lithium bromide LiBr solution as a working fluid. They started their simulations with 2D and 3D model's comparison, it was concluded that 2D models are not good enough to capture wall adhesion effects as the variation in axial direction

is not incorporated. Results showed that for each  $\theta_w$  there is a minimum value of  $Re_f$  at and above which tube is completely wetted or wetting ratio WR (which is defined by ratio between wetted area and total area) is 1. Below this minimum value of  $Re_f$ , decrease in  $Re_f$  causes film to cover less area and WR decreases. Ji et al. [56] investigated the effects of wall adhesion contact angle for different liquid load. They used VOF model to capture liquid–gas interface. They found that contact angle affects wettability considerably and higher contact angle leads to reduced wettability and increased time to reach steady-state conditions.

Ding et al. [44] investigated the effect of wall adhesion by changing contact angle to fixed values, that is, 30° and 60°, respectively, and dynamic values based on advancing and receding contact angles. It was found that wall adhesion significantly affects wettability. As the contact angle increases, inertia force increases which limits the liquid spread due to surface tension force in the axial direction and decreases elongation distance for the same liquid load. The effect on film thickness due to shrinkage of wetted area was not reported. The initial conditions may also affect the final wetted state as fully wetted state was observed when initial conditions were set to fully wetted however when zero initial conditions were set, partial wetted state was obtained. They also used dynamic contact angle modeling and found that liquid film covers most of the tube as compared with fixed contact angle modeling. It was deduced that dynamic modeling would represent realistic scenario.

Thus, it is quite evident from these studies that wall adhesion plays an important role in wettability and heat transfer. The hydrophilic materials (lower contact angle) are suited for boiling and evaporation applications, while hydrophobic materials (higher contact angle) are adopted for condensation applications [74]. Lower values of contact angle results in enhanced wettability and lower susceptibility to dry patches. Static, advancing and receding angles are different from each other [75,76] and contact angle is also affected by temperature [77]. Therefore, it is needed to compare different methodologies (fixed and dynamic contact angle values) with experimental data of wettability, to ensure which modeling will leads to accurate results. There are some CFD studies such as by Liu et al. [78], in which droplet dynamics via numerically and experimentally are compared and was found in good agreement. However, in this study only droplet dynamics have been discussed excluding wettability. The experimental and numerical evaluation of dynamic contact angle and its influence on wettability is lacking in the literature.

### 3.2. Effect of vapor flow

In horizontal falling film exchangers, liquid film that forms on tube surface is very thin and usually a fraction of millimeter. Heat and mass transfer mechanisms such as evaporation, absorption and generation depend on this thin falling film. If this film formation is disturbed by any means, the efficiency of heat exchanger will be affected. Gaseous flow influences film thickness which is inversely proportional to local heat transfer coefficient as reported in the literature [67,68,79]. Heat and mass transfer may be enhanced by gas flow as it creates waves on film surface

causing turbulence within the liquid layer as reported in the study by Gonzalez et al. [80]. In MED evaporators, vapors are generated by evaporation and flashing and all vapors are directed to next evaporator via demister and vapor route. Vapor velocity near evaporator exit may reach up to 8 m/s [81], which is high enough to cause instability in film formation, dry patches and brine carryover at lower rows of evaporator. There can be co-current and cross flow types of vapor in MED evaporator as shown in regions 4 and 5 of Fig. 3.

Ji et al. [82] experimentally investigated counter current effects on heat and mass transfer in falling film evaporator for refrigerant R-134a. It was found that heat transfer may increase or decrease depending on the tube location. Yung et al. [83] studied liquid entrainment in vapors moving in cross flow. They defined actual deflection angle  $\Upsilon$  representing droplet and jet inclination and critical deflection angle  $\Upsilon_c$  above which liquid film does not impinge over next tube as shown in Figs. 9a and b.  $\Upsilon$  and  $\Upsilon_c$  can be evaluated by:

$$\Upsilon_c = \tan^{-1} \left\{ \frac{1}{2} \left[ \frac{\phi}{d} \left( \frac{\phi}{d} - 1 \right) \right]^{-1/2} \right\} \quad (16)$$

$$\Upsilon = \tan^{-1} \left\{ \frac{1}{3} \frac{\rho_g}{\rho_l} \frac{u_g^2}{d_{dp} g} \right\} \quad (17)$$

where  $d_{dp}$  is the droplet diameter and  $\phi$  is pitch.

If  $\Upsilon < \Upsilon_c$ , liquid film falls over next tube but wetting ratio may be affected. If  $\Upsilon > \Upsilon_c$ , liquid film will not fall over next tube and probability of liquid entrainment will be high. With If  $\Upsilon = \Upsilon_c$ , critical velocity  $u_g$  can be calculated for tube arrangement and design purposes. In another study by Zhao et al. [84], vapor cross flow over refrigerant R-134a evaporator were examined. The vapor velocity was varied from 0 to 2.4 m/s for heat flux ranging from 20 to 60 kW/m<sup>2</sup> under different liquid load conditions. For lower liquid loads, heat transfer coefficient was found to remain constant and then decreases for reduced liquid load.

In an experimental and CFD study conducted by Li et al. [48], counter current gas flow was introduced to laminar falling film flow over horizontal tubes. Liquid flow was fed from top through 28 holes of  $d = 1.5$  mm, 7 mm apart and gas flow was fed from bottom via air compressor. The model was validated qualitatively with flow patterns captured in experiments and quantitatively with transitional  $Re_f$  between flow patterns. The maximum deviation from experimental and CFD transitional  $Re_f$  was less than 10%. Air velocity was varied from 0 to 0.5375 m/s and it was found that the flow pattern transitional  $Re_f$  and film thickness are affected by gas flow rate. The counter current gas flow assists and stabilizes liquid film because it counter acts gravitational effects; which results in lower liquid film velocities and thicker film due to more residence time over tube. Gas flow also affected thinnest film thickness position from 90°–100° to 70°–80°. They concluded that droplet mode is transient in nature as it has more effect of gas flow, jet and sheet modes are steadier and sheet mode has minimal effect of counter current gas flow. Fiorentino and

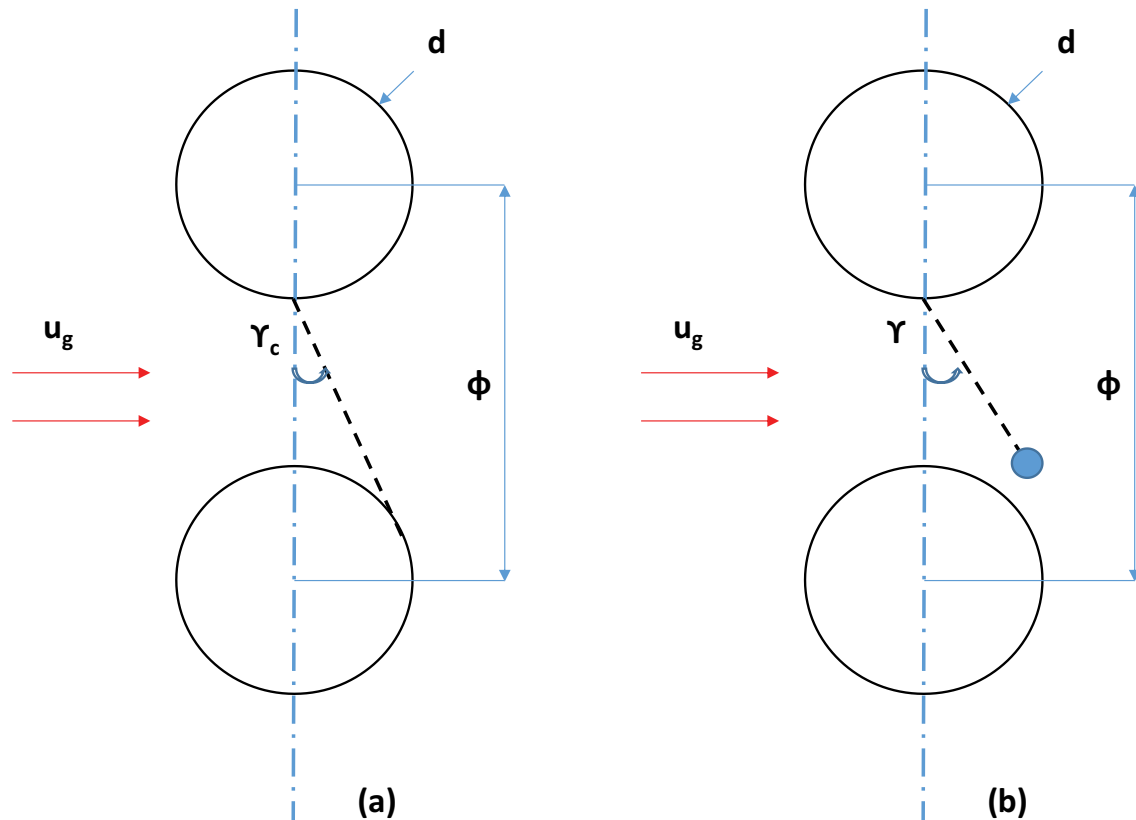


Fig. 9. Falling film deflection by vapor cross flow (a) critical deflection angle (b) actual deflection angle.

Starace [33] investigated effect of counter current moist air on falling film stability in an evaporative condenser. In this type of falling film condenser, refrigerant flows inside tube and losses heat to water film. This heat transfer mechanism allows part of water to give off vapors, which are swept by counter current airflow. They found that mass flow rates and bundle configuration should be optimized for film stability. An increase of 73% in vertical pitch requires 66.7% more water mass flow rate for film stability and to avoid film break up.

As shown in Fig. 3, there are two types of flow affecting falling film co-current and cross flow. Both of which may disturb film formation, thickness, entrainment and deflection. Numerical studies characterizing vapor flow and its effects are lacking in the literature and need to be studied in detail as it may quantify entrainment and provide limitations for MED design and operating conditions.

### 3.3. Spray system and bundle arrangement

Industrial-scale evaporators are equipped with solid cone spray nozzles for liquid load distribution. Number of nozzles are selected on the basis of evaporator size, nozzle to first row height, solid cone angle and nozzle spacing [85]. Zeng et al. [27,86] experimentally investigated performance of standard and wide angle nozzles for ammonia spray evaporators. Spray evaporation was found to be close for both cases, which shows minimal effects of cone angle. Since numerical modeling of atomization, droplets propagation

and coalescence is computationally expensive, single droplet model for spray evaporation in MATLAB was developed by Chen et al. [28]. The model was validated against 14 experimental data groups with  $\pm 12\%$  error. It was concluded that smaller droplet diameter and higher initial velocity lead to better performance. However, smaller droplet and higher velocity require higher injection pressure and pumping power, so droplet diameter of 0.5 mm was recommended to achieve better thermal utilization with an adequate pumping pressure of  $\leq 2$  bar.

Mabrouk et al. [81] developed a mathematical model using visual design and simulation software [14]. This model was used to evaluate liquid load maldistribution,  $\text{CO}_2$  release and scale formation for different bundle configurations. It was assumed that liquid spray before reaching tubes has uniform mass flux, all tubes are heated with constant heat flux and scale deposition is constant around one tube. Triangular  $60^\circ$  is the most common configuration used in industrial MED evaporators due to its compactness, overall efficiency and lower footprints. Therefore, this configuration was considered as a base study and they distinguished two types of liquid load, that is, columns based on first row (odd number) and columns based on second row (even number) as shown in Fig. 3. They found that liquid load on odd and even number rows varied significantly, and this maldistribution can be expressed as follows:

$$\frac{\Gamma_2}{\Gamma_1} = \left( \frac{\phi}{d} - 1 \right) \tag{18}$$

Above expression shows that tube configuration with a pitch of  $\phi = 1.3$  d, even number rows receive 70% less liquid load as compared with odd number rows and all tubes receives equal liquid load when the tube configuration is either square or with pitch  $\phi = 2$  d. Their results showed that doubling the liquid load reduces scale deposition by 15%. Also, scale deposition for tube configuration with  $\phi = 2$  d is 30% less as with tube configuration  $\phi = 1.3$  d.

A simplified 2-D study was carried out by Tahir et al. [85] to evaluate liquid load over columns based on first and second row, in an evaporator with triangular pitch configuration. In this study, effect of mass flow rate, number of nozzles, nozzle spacing, cone angle, nozzle to 1st row height on liquid load was evaluated. Liquid load over column based on second row was found to be less than liquid load over column based on first row. So due to maldistribution and reduced liquid load, column based on 2nd row will be more susceptible to dry patches and fouling. Their results align with the study carried out in Mabrouk et al. [81]. However, maldistribution inside tube through vapor route and outside tube due to uneven liquid load distribution still need to be addressed.

The commercial MED plant normally operates from 65°C to 40°C depending upon ambient conditions. With the incorporation of AdVC, the lower temperature can go up to 5°C and TBT can be increased up to 85°C [87–89]. From TBT to last effect temperature, thermophysical properties such as viscosity, surface tension, thermal conductivity and specific heat capacity will change and the change in properties could affect film distribution and heat transfer. For each effect operating under same liquid load and temperature difference, heat and mass transfer could be different and need to be considered for research and development. For wall adhesion, dynamic contact angle would give better results as was suggested in the study by Ding et al. [44] but wetting ratio from experiments should be compared with numerical work to conclude which methodology can lead to realistic results. In addition, contact angle dependency on temperature [77] need to be incorporated. Vapors generated in the MED evaporator flow downward and in cross flow directions. These vapors exert shear force on falling film surface, which may induce waviness and turbulence. These disturbances could affect film distribution and thermal boundary layer within the film. Therefore, effects of vapor flow need to be studied numerically for quantification of above-said phenomena. There are four types of entrainment that may exist in falling film evaporator, namely splashing, nucleate boiling, deflection and stripping [83]. Splashing is related to high liquid load. Nucleate boiling happening takes place when heat flux is high. Chances of both splashing and nucleate boiling processes are low for MED evaporator with TBT  $\leq 65^\circ\text{C}$ , low liquid load and heat flux. Nevertheless, nucleate boiling may occur for higher TBT  $> 65^\circ\text{C}$ . Stripping and deflection become important at the lower section of bundle where vapor velocity is high and need to be investigated. There are two kinds of maldistribution in MED evaporators; one is the liquid load distribution due to spray system and bundle configuration [81,85] and other is vapor flow rate inside tubes. Vapors generated in MED effect flow to next effect via vapor route. These vapors enter inside tube of next effect as a heating medium and each tube has different

vapor flow in practical scenario that can cause uneven heat flux in the bundle. Hence, optimizing liquid load and vapors distribution is of quite importance as performance and sizing of evaporator depend on this maldistribution.

#### 4. Heat and mass transfer characteristics

There are different heat and mass transfer modes in falling film around the tube in MED evaporator as shown in Fig. 10. Steam flows inside the tube and condenses by transferring heat to the film on the outer tube side. This amount of heat raises film temperature, and when the film temperature is equal or more than saturation temperature, vapors are generated via evaporation. These vapors are gathered and exit from the evaporator to the next effect for the heating purpose. Overall heat transfer coefficient  $U$  depends on several thermal resistances/heat transfer modes in falling film [20,51,60,90], which are as follows:

- Steam inside tube transfers heat by convection mode.
- Due to heat transfer, some of the vapors condense and form thin liquid film around tube, which acts as thermal resistance that include both conduction and convection heat transfer. The convection part of condensate film may be neglected.
- Heat is then transferred through tube wall by conduction, so thinner wall with high conductivity represents lower thermal resistance. If the heat flux is high, nucleate boiling may occur at tube surface but in case of MED operating conditions, heat flux is small enough to neglect nucleate boiling.
- As the falling film is flowing around tube, it gets heated by conduction and convection mode. The convection mode is often not considered, as it is insignificant as compared with film conduction thermal resistance. At the film vapor interface, evaporation starts if  $T \geq T_{\text{sat}}$ .
- Overall heat transfer coefficient may be affected by vapor flow in co-current and cross direction at the lower portion of tube bundle. However, in the upper and middle part, convection heat transfer by vapor flow may be neglected.

Numerical studies based on VOF model for heat and mass transfer are listed in Table 8 and studies based on semi-empirical or distributive parameter model are listed in Table 9. The heat and mass transfer section is further divided into seawater (desalination) and LiBr applications. LiBr-based falling film absorber and generator are currently being used in refrigeration industry. However, for MED-AVC, LiBr absorber and generator can be coupled with MED for enhanced gain output ratio [3].

##### 4.1. Seawater applications

Researchers have performed experiments on plain and enhanced tubes for falling film applications [18,19,91–93]. Enhanced tubes are more thermodynamically superior to plain tubes due to more heat transfer area and turbulence within the liquid film. But the scaling problem limits the use of enhanced tubes in MED evaporators [51]. Heat transfer in these evaporators strongly depends on film Reynolds

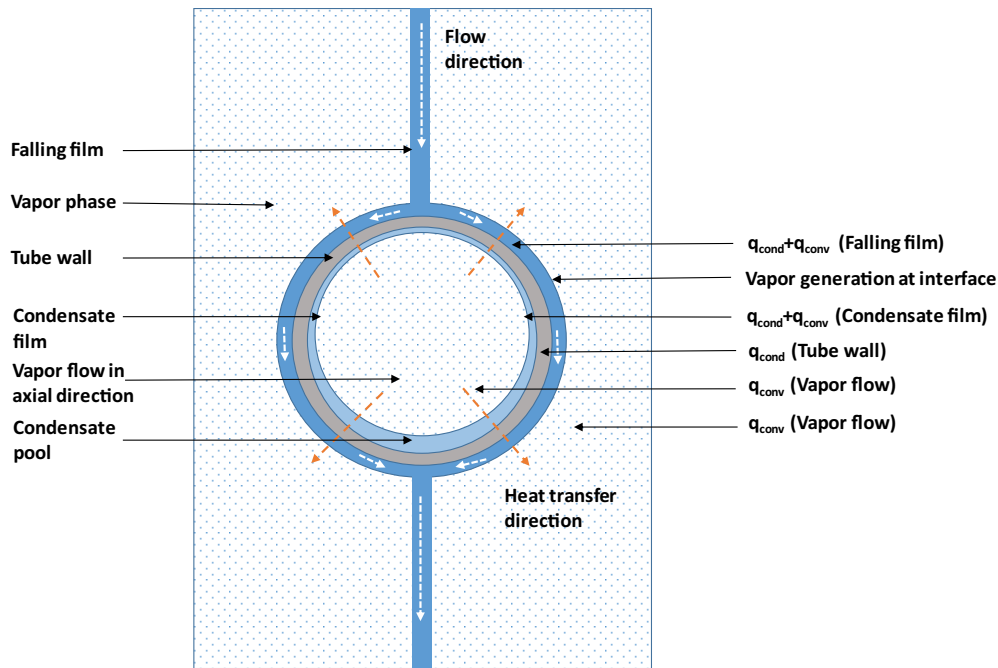


Fig. 10. Heat and mass transfer in a falling film flow.

number, flow pattern, inter-tube spacing and thermophysical properties [6,15]. For a single falling film tube experiments, falling film heat transfer coefficient decreases with an increase of liquid load [25,64,94]. Xu et al. [79] came to conclusion that the overall heat transfer coefficient increases with an increase in liquid load. They performed experiments for a wide range of film Reynolds number, that is,  $Re_f = 200-2,500$ . In contrary, Zeng et al. [25] found minimal effects of liquid load on overall heat transfer coefficient. Newson [95], Slesarenko [96], and Yang and Shen [97] found insignificant effect of salinity in heat transfer coefficient. However, Fletcher et al. [98] concluded a decreasing trend of heat transfer coefficient when shifted from fresh water to seawater. With respect to heat transfer, there are four regions in falling namely stagnation, impingement, thermal developing and thermally developed based on thermal boundary layer [99]. Local heat transfer coefficient is expected to be high in first three regions due to high thermal gradients as compared with fully developed region. In MED falling film evaporators, mostly vapors generated in the upper section by flashing and in the middle and lower section of evaporator by conduction/convective heat transfer. Evaporation dominates instead of nucleate boiling in these evaporators due to low heat flux conditions. Mitrovic [100] calculated the temperature limit above which nucleate boiling starts and below which evaporation dominates. If by any means, nucleate boiling occurs, it may lead to dry patches and scale formation due to nucleation and bubble growth in the falling film. The effect of high TBT needs further investigation for nucleate boiling, liquid load and scale formation.

For microscopic understanding of heat and mass transfer, numerical studies have been carried out. Jin et al. [101] developed a mathematical model and concluded that tube with constant heat flux boundary condition would provide 12%

enhanced heat transfer coefficient as compared with tube with constant temperature boundary condition. Kouhikamali et al. [102] used Eulerian multiphase model coupled with Lee evaporation model [39] to quantify heat transfer coefficient, vapors generation and pressure drop for different tubes arrangement and operating conditions. Results showed rise in temperature difference would increase heat transfer coefficient, pressure drop and evaporation. Furthermore, vertical array was found to be more effective than horizontal array. Bigham et al. [103] have reached similar conclusion by using VOF model and Lee model, considering the flow is turbulent; that higher temperature difference and feed flow rate leads to higher heat transfer coefficient and evaporation rate. However, in MED plants, the temperature difference depends on number of effects and usually in the range of  $3^{\circ}\text{C}-5^{\circ}\text{C}$  [8,12,104]. Yang et al. [105] evaluated heat transfer coefficient and axial temperature distribution along the tube by coupling external film distribution with internal condensation. They developed 2D numerical code in which phase change mass transfer was evaluated by:

$$\dot{m}_{l \text{ or } g} \times H_{lg} = -k \left. \frac{\partial T}{\partial y} \right|_{\text{int}} \quad (19)$$

It was concluded that performance could be optimized by controlling liquid load as per internal condensation variation. Internal condensation was also taken in account by Zhou et al. [47] for falling film evaporation. They modeled 14 mm diameter tube with 1 mm thickness in the axial direction in 3D domain. Numerical results showed that overall heat transfer coefficient mainly depends on internal heat transfer coefficient and internal heat transfer coefficient increases inside tube as steam condenses. In addition, liquid

Table 8  
CFD studies for falling film heat and mass transfer using VOF method

Studies	Domain	Working fluid	Assumptions	Flow mode	Parameters varied	Parameters observed	Key findings
Abraham and Mani [60,106]	(i) Single tube (ii) 5 tubes column $d = 25.4$ mm	Water + water vapor	$T_w = 64.6^\circ\text{C}$ , $T_f = 58.6^\circ\text{C}$ , $T_{\text{sat}} = 62.6^\circ\text{C}$	-	$Re_f = 173-1,250$ $d = 19.05, 25.4$ & $50.8$ mm, $T_{\text{sat}} = 59.6^\circ\text{C}-63.6^\circ\text{C}$ $v = 0.071-0.15$ m/s $T_f = 58^\circ\text{C}-61^\circ\text{C}$	$h$ , $\dot{m}_{\text{vap}}$	Staggered configuration has 31% less evaporation than in-line configuration due to less $U$
Yang et al. [51]	2 tubes $O = 1$ mm, $d = 25.4$ mm, $h_f = 5$ mm	Water - air	Constant TPP, $T_w = 62^\circ\text{C}$ , $T_{\text{sat}} = 60^\circ\text{C}$ $\theta_w = 0^\circ$	-		$h$ .	Enhanced heat transfer at $\theta = 5^\circ$ due to the presence of laminar sublayer. In this laminar sublayer, convection heat transfer dominates
Hosseinnia et al. [43]	3 tubes $O = 1 \times 1$ mm <sup>2</sup> , $d = 19.05$ mm, $s = 24.5$ mm, $L = 20$ mm, $h_f = 2$ mm	LiBr sol + water vapor	Constant TPP, $T_w = 30^\circ\text{C}$ , $T_f = 47^\circ\text{C}$	D, J	$\Gamma_{1/2} = 0.03$ & $0.0615$ kg/m-s	Water vapor absorption rate	Average vapor absorption rate decreases by one order of magnitude when flow regime changed from droplet to jet mode
Zhao et al. [90]	Same as Zhao et al. [45]	Water + air	$q = \text{constant}$ , $\theta_w = 10^\circ$ , Laminar	-	Same as [45] + $q = 1-100$ kW/m <sup>2</sup>	$h$ .	New correlation for $h$ was developed based on $\Gamma_{1/2}$ , $d$ , $q$ , $h_i$ and $T_{\text{inlet}}$
Qi et al. [50]	Elliptical tube $L = 18$ mm, $O = 1.5$ mm	Seawater + air	Constant TPP, $q = 0$ , $\theta_w = 30^\circ$ , $T_w = 71.2^\circ\text{C}$ , turbulent	D, D-J, J	$\Gamma_{1/2} = 0.037, 0.093$ and $0.149$ kg/m-s Shape factor $E = 1-2.1$	$\delta$ , $h$ .	$h$ of elliptical tubes with ellipticity = 1.5 was 20%-22% more than that of circular tubes
Luo et al. [112]	Circular tube $d = 19$ mm, $wd = 1$ mm	Water + water vapor	Constant TPP, Laminar, $T_w = 62^\circ\text{C}$ , $T_f = T_{\text{sat}} = 60^\circ\text{C}$	-	$\Gamma_{1/2} = 0.2, 0.29, 0.29$ & $0.49$ kg/m-s, round, drop and oval shape, $h_i = 6-15$ mm	$\delta$ , $h$ .	$\delta_{\text{min}}$ for drop and oval shaped are 2% and 9.8% less as compared with circular tube respectively. $h$ for drop and oval shaped are 12.6% and 34% higher as compared with circular tube, respectively
Zhou et al. [47]	One tube $d = 14$ mm domain = $15 \times 30 \times 1$ mm <sup>3</sup>	Water + water vapors	Constant TPP at $T_{\text{avg}}$ Laminar, $T_f = 60^\circ\text{C}$ , $T_s = 65^\circ\text{C}$ , $\theta_{\text{in}} = 20^\circ$	S	$\Gamma_{1/2} = 0.279, 0.349$ & $0.437$ kg/m-s	$\delta$ , $h$ , $q$ .	$\Gamma_{1/2}$ has minimal effect on $h_{\text{in}}$ . $U$ mainly depends on $h_{\text{in}}$
Bigham et al. [103]	Two tubes	Water + water vapors	Constant TPP, turbulent, $T_{\text{sat}} = 48.5^\circ\text{C}$	-	$\dot{m}_f = 0.001-0.03$ kg/s, $\Delta T = 4.75^\circ\text{C}-38^\circ\text{C}$	$h$ , $\dot{m}_{\text{vap}}$	Rise in $\dot{m}_f$ and $\Delta T$ increases $h$ & $\dot{m}_{\text{vap}}$
Subramaniam and Garimella [54,55]	One tube $d = \varphi = 15.9$ mm,	LiBr sol (65%wt.) + water vapor	Laminar, $T_f = 40.5^\circ\text{C}$ , $T_w = 30^\circ\text{C}$ , $\Gamma_{1/2} = 0.0086$ kg/m-s	D	$t$	$h$ , mtc, $C$	As the droplet impacts on tube, it causes solution to mix and concentration at film surface becomes high that enhances heat and mass transfer mechanisms

D = droplet, J = jet and S = sheet.

Table 9  
Numerical studies for falling film heat and mass transfer, implemented models other than VOF

Studies	Details and numerical method	Assumptions	Parameters varied	Parameters observed	Key findings
Hou et al. [6]	$d = 25.4$ mm, $d_{in} = 24$ mm $L = 10$ m, triangular array 152 tubes (1st pass) 21 tubes (2nd pass)	Steady process, effects of crossflow and fouling are neglected, uniform $\Gamma_{1/2}$ .	$T_f = 40.2^\circ\text{C}$ – $58.6^\circ\text{C}$ $\dot{m}_f = 331$ – $357$ ton/h, $\dot{m}_s = 8.28$ – $125.96$ ton/h	$h$ , $\Gamma_{1/2}$ , $X$	Steam is not uniformly distributed. $\Gamma_{1/2}$ decreases from top to bottom row due to evaporation and non-uniformity
Azimibavil and Jafarian Dehkordi [118]	$d = 28.575$ mm, $L = 4.5$ m Tubes = 59 rows $\times$ 100 columns, $T_s = 68^\circ\text{C}$ , $\dot{m}_s = 11.84$ kg/s, $T_f = 44^\circ\text{C}$ , $\dot{m}_f = 35.44$ kg/s	Laminar, uniform $\Gamma_{1/2}$ , $\Delta P = 0$ (inside tube), modeling of one column is enough to represent all columns.	$t = 0$ – $1,200$ s	$\dot{m}_{vap}$	If feed is cut by half of its nominal value at any time, then brine salinity may increase more than design limit and tubes will be more susceptible to fouling
Gong et al. [117]	$d = 25.4$ mm, $L = 8$ m, tri array, 12,012 tubes (1st pass) 1,560 tubes (2nd pass) $T_s = 63^\circ\text{C}$ , $\dot{m}_s = 27.8$ kg/s $T_f = 40^\circ\text{C}$	Uniform $\Gamma_{1/2}$ at top, fouling effects are neglected, steam is fully condensed at the end of 2nd pass, inter-tube vapor flow is cross flow	$\Gamma_{1/2} = 0.05$ – $0.09$ kg/m-s $X = 30,000$ – $50,000$ ppm	$h$	$h$ is higher in evaporating zone as compared with pre-heating zone
Kouhikamali et al. [102]	$d = 28.57$ mm Vertical array: $\varphi_y > \varphi_x$ Horizontal array: $\varphi_x > \varphi_y$	Wall effects are neglected, turbulent flow, mixture properties	$\varphi_y$ & $\varphi_x$	$h$ , $\Delta P$ , $\dot{m}_{vap}$	$h$ increases when $\Gamma_{1/2}$ increases or $X$ decreases Vertical array provides better $h$ and $\dot{m}_{vap}$ than horizontal array
Louahlia-Gualous and El Omari [119]	$d = 50$ mm, $d_{in} = 16$ mm, $h_i = 19$ mm, $L = 140$ mm,	$\delta \ll d$ , constant TPP, 2D with axisymmetric, co-current airflow, sheet flow	$\Gamma_{1/2}$	$h$ , $\dot{m}_g$ , $\delta$	Increasing $\Gamma_{1/2}$ enhances $h$ and reduces $\dot{m}_g$
Wunder et al. [61]	$d = 38$ mm, $d_{in} = 35$ mm, $s = 10$ mm	$\delta \ll d$ , constant TPP, laminar, heat transfer is only by conduction, tube is fully wetted and stratified flow of condensate inside tube	$s$ , $\Delta T$ , $d/L$	$\delta$ , $h$ , $\Delta P$ , $U$	As $\Delta T$ increases, vapors condense faster which thickens condensate $\delta$ and decreases $U$ Optimum $d/L$ ratios were evaluated for better $U$

load has minimal effect on internal heat transfer coefficient. The phase change models for evaporation outside tube and condensation inside tube were not incorporated and discussed. Abraham and Mani [60] conducted both experimental and numerical studies on in-line and staggered tube, falling film configuration. In their set-up, evaporator was equipped with 15 tubes (3 columns and 5 rows). CFD results showed that staggered configuration has 31% less evaporation than in-line configuration due to less overall heat transfer coefficient. However, from their volume fraction contours, falling film is not formed except for the first tube and it shows splashing which is contradictory to other studies. Therefore, overall evaporation results may differ if the film is formed completely. In addition, details for evaporation model were not provided. In their another study by Abraham and Mani [106] flame coated spray was used to control surface roughness and it was found that heat transfer coefficient increases as roughness increases but after certain roughness values, heat transfer coefficient decreases.

Usually, in modeling falling film heat transfer mechanism, it is assumed that the temperature profile within the liquid layer is linear causing heat transfer mode to be mainly conduction and convection effects are usually neglected [107,108]. However numerical study by Yang et al. [51] showed enhanced heat transfer at  $\theta = 5^\circ$  due to the presence of laminar sublayer. Laminar sublayer was distinguished from laminar flow with the help of normal velocity profile within the film. This sublayer causes turbulence within the film that leads convection heat transfer to dominate and results in improved overall heat transfer. The laminar sublayer diminishes as the inclination angle increases. In a CFD study by Zhao et al. [90], effects of subcooled falling film on heat transfer coefficient were investigated. As the falling film was considered subcooled, phase change mass and heat transfer were neglected. They found that heat transfer coefficient on smaller tube diameter is higher than that of larger tube diameter because thermal boundary develops faster in larger tube diameters. They developed heat transfer coefficient correlation using 141 cases for different liquid load  $\Gamma_{1/2}$ , viscosity  $\mu$ , tube diameter  $d$ , surface tension  $\sigma$ , inlet temperature  $T$ , heat flux  $q$  and impingement height  $h_i$ . However, the correlation only accounts for subcooled conditions and evaporation effects are neglected. This correlation may be used for upper part of evaporator where evaporation can be neglected. Furthermore, the author tried to reproduce the correlation but it showed decreasing trend with increasing  $Re_f$  as it should have shown increasing trend as per their results and comparison. This may be due to typo mistake in correlation.

Apart from circular tubes, tubes with other geometries have also been considered for falling film applications. Evaporators with elliptical tubes have been studied for air conditioning, chemical and refrigeration industries [109–111]. Qi et al. [50] evaluated heat transfer coefficient for elliptical tube in seawater desalination application. They implemented VOF model and phase change effects were not considered. In their experimental and numerical work, film formation on elliptical tube with ellipticity = 1.5 was found to be faster than circular tube. Rapid film formation causes thinner and even distribution, which results in enhanced heat transfer coefficient 20%–22% more than circular tubes.

In another study, drop and oval shaped tube performances were compared with circular tube numerically [112]. Drop and oval shaped tube was found to have thinner thermal boundary layer and heat transfer coefficients were 12.6% and 34% higher as compared with circular tube, respectively. To author's knowledge, tubes other than circular geometry have not been commercially used for MED evaporators and need more in-depth study for feasibility. A rotating tube is an enhanced tube which gives higher heat transfer rates as compared with fixed tubes in falling film applications [113,114]. Lin et al. [115] conducted experimental and CFD analysis (VOF model) on radially rotating tube for offset angle characterization, which may affect heat transfer coefficient. The analysis showed that when the counter clockwise rotation is increased from 0 to 400 rpm, liquid film on the left hand of column gets thinner as compared with right hand side and offset angle decreases. This can cause asymmetric film profile along vertical plane and resulting in better heat transfer coefficient on one side of tube. This type of tube configuration may not be feasible for desalination application as asymmetric liquid load distribution may increase dry patches. Also, MED evaporator consists of tubes in thousands and cost for developing these tubes will be very high due to rotating system which makes these tubes not feasible for desalination application.

As the VOF model limits to study only fewer tubes in detail because of computational cost and time, to characterize whole bundle, researchers have applied semi-empirical and distributive models. In these models, whole domain is discretized into small elements and global conservations of mass, momentum, energy are solved for each element. Hou et al. [6] used distributive parameter model (DPM) for designing and optimizing falling film evaporator performance used in MED plants. In this 2D model, general conservation equations along with correlations are implemented instead of differential conservation equations, Chato's [116] correlation was used to evaluate two-phase flow heat transfer coefficient. Results showed maximum overall heat transfer coefficient of 3,300 W/m<sup>2</sup>-K was observed at the entrance of tube and then decreases gradually in the axial direction. The average overall heat transfer coefficient of evaporator was 2,800 W/m<sup>2</sup>-K. Liquid load decreases from 0.063 kg/m-s to minimum value of 0.04 kg/m-s due to evaporation and non-uniformity. Gong et al. [117] simulated 3-D modeling of horizontal falling film evaporator with aluminum-brass tubes in triangular configuration. They used DPM with empirical correlations to quantify heat transfer coefficient variation with respect to liquid load, salinity and along tube row, column and length direction. It was shown that heat transfer coefficient increases as liquid load increases or salinity decreases, while condensation heat transfer coefficient was found insensible to liquid load. Heat transfer coefficient was higher for preheating zone (2nd pass) as compared with evaporating zone (1st pass). Azimibavil and Jafarian Dehkordi [118] developed in-house code and analyzed transient process of MED evaporator during startup till it reaches steady-state condition. They solved simplified differential equations along with the correlations available in the literature for one column. In their modeling, they assumed that all columns have same heat and mass transfer characteristics, so modeling of one

column is enough to represent all columns and tube can be considered as vertical wall instead of cylindrical wall for the sake of simplicity. They found that if feed is cut by, half of its nominal value at any time, then brine salinity may increase more than design limit and tubes will be more susceptible to fouling. Louahlia-Gualous and El Omari [119] developed numerical model based on finite difference method to compute boundary layer thickness, heat transfer coefficient and evaporation rate. In their model, co-current airflow rate with was assumed to be in contact with film. Conservation equations of mass, momentum and energy were developed for each phases and modified for presented problem. Evaporation rate was computed by energy balance at the interface. In longitudinal direction, backward difference was adopted and in radial direction, central difference was adopted for velocity, mass fraction and temperature. These equations were solved along with evaporation model in a marching manner. Numerical results showed that rise in liquid load enhances heat transfer coefficient and decreases evaporation rate. Lately, Wunder et al. [61] developed 3D model of one tube using semi-empirical method. They considered both heat transfer mechanisms; steam condensation inside tube and film evaporation outside tube via conduction mode. It was observed that when the temperature difference increases condensation process enhances, which thickens the condensate film inside tube; this causes overall heat transfer coefficient to decrease. In addition, they evaluated different tube diameter to length ratios for better overall heat transfer coefficient. These semi-empirical studies are quicker and whole domain can be analyzed. However, simplified assumptions such as negligible effects of vapor flow and liquid load uniformity with the accuracies of film and heat transfer correlations may reflect some inconsistencies in the solution.

This section concluded that numerical studies for seawater applications are still limited, as more insight is needed to develop better understanding of falling film evaporators. VOF model is used in some studies, which is computationally expensive, only small part of domain can be analyzed, other used empirical correlations to examine whole domain but the accuracy of surface tracking/film thickness, and evaporation rate is limited which varies from one correlation to other. However, some researchers developed in-house modified CFD code as a tradeoff between accuracy and computational time but these models are specific to certain geometry and operating conditions. Furthermore, the accuracy of evaporation model (specially Lee [39] model), effect of non-condensable gases, nucleate boiling, effects of CO<sub>2</sub> release and vapor flow on evaporation are some research gaps that is still need to be addressed. Substantial experimental work has been carried out to assess CO<sub>2</sub> release and scale formation/fouling [71,120,121] in horizontal falling film evaporator used in desalination plants. Three main salts namely calcium carbonate (CaCO<sub>3</sub>), magnesium sulfate (MgSO<sub>4</sub>) and calcium sulfate (CaSO<sub>4</sub>) present in seawater, participates in scale deposition. There are zero dimension models available in the literature addressing CO<sub>2</sub> release and scale formation [81,104,122]. CFD models need to be developed for CO<sub>2</sub> release and fouling in falling film evaporators; and how this mass transfer and deposition may affect falling film hydrodynamics and heat transfer mechanism.

A CFD model for CaCO<sub>3</sub> deposition [123] in internal flows is available in the literature that might help researcher to implement or modify for particular application.

#### 4.2. Lithium bromide (LiBr) falling film applications

For numerical model development of LiBr falling films, Min and Choi [124] examined surface tension effects by solving conservation equations in dimensionless form for water vapor absorption in LiBr solution. Incorporation of surface tension modeling was recommended to accurately predict mass transfer process in falling film absorber. Ouldhadda et al. [125] developed falling film model for Newtonian and non-Newtonian fluids by solving conservation equations using implicit finite difference scheme. Giannetti et al. [126] established analytical solutions for heat and mass transfer coefficients of LiBr absorption on a partially wetted horizontal tube. They assumed constant wall temperature, small impingement zone, very small  $\delta$  as compared with tube diameter and tube length, laminar flow and negligible heat transfer to environment for their solution developed. Analytical results were compared with numerical [127] and experimental results [128,129] available in literature and were found in good agreement.

Subramaniam and Garimella [54,55] developed 3D CFD model to address falling film heat and mass transfer processes. They modeled one tube of 15.9 mm diameter with constant temperature at wall and periodic conditions at inlet/outlet for LiBr solution baser absorber. They evaluated heat and mass transfer coefficients of LiBr solution drop at different stages and found that during drop impact on tube, solution is mixed and concentration on the film surfaces becomes high which enhances heat and mass transfer mechanism. Chen et al. [130] conducted CFD analysis of mesh guider inserts in a staggered tube bundle for vapor absorption in LiBr solution. The purpose of using mesh inserts was to avoid uneven liquid load distribution and results showed that heat and mass transfer coefficient were 33.4% and 55.4% higher than that of plain tube. Hosseinnia et al. [43] studied water vapor absorption in LiBr solution over horizontal tubes using in-house CFD code. Two falling film regimes, droplet and jet mode were considered to address this combined heat and mass transfer problem. The CFD model was compared with experimental data and numerical model presented in the literature [63,131], respectively, and the results were found to be in good agreement. The amount of vapor absorbed and heat of absorption were evaluated by using Fick's law.

$$\dot{m}_{\text{abs}} = -\frac{\rho D}{C_{\text{int}}} \times \frac{\partial C}{\partial n} \Big|_{\text{int}} \quad (20)$$

$$q_{\text{abs}} = H_{\text{abs}} \times \dot{m}_{\text{abs}} \quad (21)$$

The initial concentration of LiBr solution was 0.6 but as it absorbed vapors, heat of absorption is released and transferred to the cooling water inside tubes. It was assumed that the heat of absorption is constant and equal to 2.74 MJ/kg. At the lower tube, the concentration reduces to 0.54 and temperature reduces to 35°C in droplet mode while

0.565 and 39°C, respectively, in jet mode. Their results showed that vapor absorption rate depends on flow regimes and average vapor absorption rate decreases by one order of magnitude when flow regime changed from droplet to jet mode.

Although, LiBr falling film evaporator can be coupled with MED to increase productivity, there is no numerical studies for LiBr-based evaporator for desalination applications. The vapor absorption rate in Eq. (20) can be modified and implemented for CO<sub>2</sub> release application. Furthermore, in MED-AVC design [3], absorber generates steam instead of using cooling water which may affect absorption rate outside tube. In principle, this can be studied numerically for improved performance.

### 5. Concluding remarks

Comprehensive and critical review focusing on CFD analyses for horizontal falling film evaporators in MED plants, and key research gaps are presented in this paper which can be summarized as:

- Experimental correlations can be used in selecting the proper CFD domain size, liquid load for particular flow mode and for comparison purposes.
- VOF model is accurate in tracking liquid–gas interface but is computationally expensive while semi-empirical or DPM models can assess larger domain but the accuracy is compromised.
- Commercial MED plants operate from TBT of 65°C to lower brine temperature of 40°C. However, there are recent works focused on working beyond this temperature limit. In this case, change in thermophysical properties with temperature would affect film distribution and heat transfer. Therefore, it is needed to evaluate falling film characteristics at different operating conditions for accurate MED evaporator design calculation.
- For wettability, researchers have used static and dynamic contact angle but CFD comparison and verification with experimental data is not available. A comparison study will provide the proper contact angle to be used for realistic results to avoid scale formation. In addition, contact angle dependency on temperature need to be incorporated.
- Zero dimension models of CO<sub>2</sub> release and scale formation are reported in the literatures; however, the CFD models need to be established which may develop better understanding of mass transfer and deposition and how it affects film hydrodynamics and heat transfer mechanism.
- Liquid load maldistribution due to nozzle spray system/bundle configuration not only affecting the variation in heat transfer coefficient and evaporation rate but also influencing the liquid load distribution among tubes and accordingly the scale deposition formation rate.
- Non-uniform vapor flow rate inside tubes may cause uneven heat flux in the tube bundle. Hence, optimizing vapors distribution is of quite importance for better evaporator performance and accurate sizing of the evaporator.
- The vapor flow in co-current and cross direction may disturb falling film flow by inducing waviness and

entrainment. Quantification of these effects using CFD will help in developing safe operating conditions to avoid abrupt heat transfer, dry patches and scale formation.

### Acknowledgments

The authors would like to acknowledge the support of College of Science and Engineering (CSE) and Qatar Environment and Energy Research Institute (QEERI) of Hamad Bin Khalifa University (HBKU).

### Conflict of interest

None

### Symbols

$A$	–	Area, m <sup>2</sup>
$AdVC$	–	Adsorption vapor compression
$Ar$	–	Archimedes number
$AVC$	–	Absorption vapor compression
$C'$	–	Constant
$C$	–	Concentration
$Co$	–	Courant number
$C_p$	–	Specific heat, J/kg-K
CFD	–	Computational fluid dynamics
CSF	–	Continuum surface force
$D$	–	Diffusivity, m <sup>2</sup> /s
$d$	–	Diameter, mm
DPM	–	Distributed parameter model
DDPM	–	Dense discrete particle model
$F$	–	Force, N
$g$	–	Acceleration due to gravity, m/s <sup>2</sup>
$Ga$	–	Modified Galileo number
GCC	–	Gulf Cooperation Council (Qatar, Bahrain, Kuwait, United Arab Emirates, Oman and Saudi Arabia)
$H$	–	Enthalpy, kJ/kg
$h$	–	Heat transfer coefficient, W/m <sup>2</sup> -K
$h_i$	–	Impingement height, mm
$K$	–	Surface curvature
$k$	–	Thermal conductivity, W/m-K
$L$	–	Tube length, mm
$\dot{m}$	–	Mass flow rate, kg/s
MED	–	Multi-effect desalination
MSF	–	Multi-stage flash
mtc	–	Mass transfer coefficient
LiBr	–	Lithium bromide
$n'$	–	Power constant
$n$	–	Unit normal direction vector at interface
NF	–	Nano filtration
$Nu$	–	Nusselt number
$O$	–	Orifice
PR	–	Performance ratio (amount of distillate produced by unit mass flow rate of steam)
$q$	–	Heat flux, W/m <sup>2</sup>
$Re_f$	–	Film Reynolds number = $4\Gamma_{1/2}/\mu$
RO	–	Reverse osmosis
$S$	–	Source term
$s$	–	Inter-tube distance – tube wall to tube wall, mm

$T$	—	Temperature, °C/K
$t$	—	Time, s
TBT	—	Top brine temperature, °C/K
TPP	—	Themophysical properties
$U$	—	Overall heat transfer coefficient, W/m <sup>2</sup> -K
$u$	—	Velocity in $x$ -direction, m/s
$V$	—	Velocity, m/s
$v$	—	Velocity in $y$ -direction, m/s
VOF	—	Volume of fluid
$w$	—	Velocity in $z$ -direction, m/s
wd	—	Width, mm
We	—	Weber number
WR	—	Wetting ratio
$X$	—	Salinity, ppm

**Greek**

$\alpha$	—	Void fraction
$\beta$	—	Mass transfer time relaxation factor
$\Upsilon$	—	Deflection angle
$\Gamma_{1/2}$	—	Liquid load-one side, kg/m-s = $\dot{m}/L$
$\rho$	—	Density, kg/m <sup>3</sup>
$\sigma$	—	Surface tension, N/m
$\Delta$	—	Difference
$\phi$	—	Tube pitch, center to center, mm
$\theta$	—	Angle of inclination, degrees
$\theta_c$	—	Solid cone angle, degrees
$\theta_w$	—	Contact angle, degrees
$\mu$	—	Viscosity, kg/m-s
$\alpha$	—	Volume fraction
$\delta$	—	Film thickness, m
$\lambda$	—	Spacing between two neighbor droplets or jets

**Subscripts**

1	—	Column based on 1st row
2	—	Column based on 2nd row
abs	—	Absorbed
avg	—	Average
cond	—	Conduction
conv	—	Convection
$c$	—	Critical
$d$	—	Distillate
dp	—	Drop
$e$	—	Energy
ex	—	external
$f$	—	Feed
$g$	—	Gaseous phase
gen	—	Generated
in	—	internal
int	—	interface
$l$	—	Liquid phase
$m$	—	Mass
min	—	Minimum
sat	—	Saturation
$s$	—	Steam
vap	—	Vapors
vol	—	Volumetric
$w$	—	Wall
$x$	—	$x$ -direction

$y$	—	$y$ -direction
$z$	—	$z$ -direction

**References**

- [1] M.W. Shahzad, K.C. Ng, K. Thu, B.B. Saha, W.G. Chun, Multi effect desalination and adsorption desalination (MEDAD): a hybrid desalination method, *Appl. Therm. Eng.*, 72 (2014) 289–297.
- [2] A. Mabrouk, A. Abotaleb, F. Tahir, M. Darwish, R. Aini, M. Koc, A. Abdelrashid, High Performance MED Desalination Plants Part I: Novel Design MED Evaporator, IDA 2017 World Congress Water Reuse Desalination, Sao Paulo, Brazil, 2017.
- [3] A. Mabrouk, A. Abotaleb, H. Abdelrehim, F. Tahir, M. Koc, A. Abdelrashid, A. Nasralla, High Performance MED Desalination Plants, Part II: Novel Integration MED-Absorption Vapor Compression, IDA 2017 World Congress Water Reuse Desalination, Sao Paulo, Brazil, 2017.
- [4] F.W. Adams, G. Broughton, A.L. Conn, A horizontal film-type cooler: film coefficients of heat transmissions, *Ind. Eng. Chem.*, 28 (1936) 537–541.
- [5] A.M.I. Mohamed, Flow behavior of liquid falling film on a horizontal rotating tube, *Exp. Therm. Fluid Sci.*, 31 (2007) 325–332.
- [6] H. Hou, Q. Bi, X. Zhang, Numerical simulation and performance analysis of horizontal-tube falling-film evaporators in seawater desalination, *Int. Commun. Heat Mass Transf.*, 39 (2012) 46–51.
- [7] M.W. Shahzad, M. Burhan, L. Ang, K.C. Ng, Adsorption Desalination—Principles, Process Design, and Its Hybrids for Future Sustainable Desalination, *Emerging Technologies for Sustainable Desalination Handbook*, Elsevier B.V., pp. 3–34.
- [8] A.N. Mabrouk, H.E.S. Fath, Technoeconomic study of a novel integrated thermal MSF–MED desalination technology, *Desalination*, 371 (2015) 115–125.
- [9] I.S. Al-Mutaz, Coupling of a nuclear reactor to hybrid RO-MSF desalination plants, *Desalination*, 157 (2003) 259–268.
- [10] G. Iaquaniello, A. Salladini, A. Mari, A.A. Mabrouk, H.E.S. Fath, Concentrating solar power (CSP) system integrated with MED–RO hybrid desalination, *Desalination*, 336 (2014) 121–128.
- [11] M. Darwish, *Desalination Engineering*, 1st ed., Balaban Desalination Publications, MA, USA, 2015.
- [12] F. Tahir, M. Atif, M.A. Antar, The Effect of Fouling on Performance and Design Aspects of Multiple-Effect Desalination Systems, *Recent Progress in Desalination, Environmental and Marine Outfall Systems*, Springer International Publishing, Cham, 2015, pp. 35–52.
- [13] A.S. Nafey, H.E.S. Fath, A.A. Mabrouk, Thermo-economic investigation of multi effect evaporation (MEE) and hybrid multi effect evaporation—multi stage flash (MEE-MSF) systems, *Desalination*, 201 (2006) 241–254.
- [14] A.S. Nafey, H.E.S. Fath, A.A. Mabrouk, A new visual package for design and simulation of desalination processes, *Desalination*, 194 (2006) 281–296.
- [15] J. Mitrovic, Influence of Tube Spacing and Flow Rate on Heat Transfer from a Horizontal Tube to a Falling Liquid Film, 8th International Heat Transfer Conference, San Francisco, 1986, pp. 1949–1956.
- [16] J.T. Rogers, S.S. Goindi, Experimental laminar falling film heat transfer coefficients on a large diameter horizontal tube, *Can. J. Chem. Eng.*, 67 (1989) 560–568.
- [17] Y. Fujita, M. Tsutsui, Experimental investigation of falling film evaporation on horizontal tubes, *Heat Transf. Jpn. Res.*, 27 (1998) 609–618.
- [18] J.-F. Roques, J.R. Thome, Falling films on arrays of horizontal tubes with R-134a, Part I: Boiling heat transfer results for four types of tubes, *Heat Transf. Eng.*, 28 (2007) 398–414.
- [19] J.-F. Roques, J.R. Thome, Falling films on arrays of horizontal tubes with R-134a, Part II: Flow visualization, onset of dryout, and heat transfer predictions, *Heat Transf. Eng.*, 28 (2007) 415–434.
- [20] J. Fernández-Seara, Á.Á. Pardiñas, Refrigerant falling film evaporation review: description, fluid dynamics and heat transfer, *Appl. Therm. Eng.*, 64 (2014) 155–171.

- [21] Y. Zheng, X. Ma, Y. Li, R. Jiang, K. Wang, Z. Lan, Q. Liang, Experimental study of falling film evaporation heat transfer on superhydrophilic horizontal-tubes at low spray density, *Appl. Therm. Eng.*, 111 (2017) 1548–1556.
- [22] J. Mitrovic, Flow structures of a liquid film falling on horizontal tubes, *Chem. Eng. Technol.*, 28 (2005) 684–694.
- [23] X. Hu, A.M. Jacobi, The intertube falling film: Part 1—Flow characteristics, mode transitions, and hysteresis, *J. Heat Transf.*, 118 (1996) 616.
- [24] J.F. Roques, V. Dupont, J.R. Thome, Falling film transitions on plain and enhanced tubes, *J. Heat Transf.*, 124 (2002) 491.
- [25] X. Zeng, M.-C. Chyu, D.Z.H. Ayub, Evaporation heat transfer performance of nozzle-sprayed ammonia on a horizontal tube, *ASHRAE Trans.*, 101 (1995) 136–149.
- [26] J. Hou, H. Cheng, D. Wang, X. Gao, C. Gao, Experimental investigation of low temperature distillation coupled with spray evaporation, *Desalination*, 258 (2010) 5–11.
- [27] X. Zeng, M.-C. Chyu, Z.H. Ayub, Experimental investigation on ammonia spray evaporator with triangular-pitch plain-tube bundle, Part I: tube bundle effect, *Int. J. Heat Mass Transf.*, 44 (2001) 2299–2310.
- [28] Q. Chen, K. Thu, T.D. Bui, Y. Li, K.C. Ng, K.J. Chua, Development of a model for spray evaporation based on droplet analysis, *Desalination*, 399 (2016) 69–77.
- [29] C. Hirt, B. Nichols, Volume of fluid (VOF) method for the dynamics of free boundaries, *J. Comput. Phys.*, 39 (1981) 201–225.
- [30] F. Tahir, A. Mabrouk, M. Koc, CFD Analysis of Falling Film Wettability in MED Desalination Plants, Qatar Foundation Annual Research Conference Proceedings, 2018, p. EEPD650.
- [31] Q. Qiu, X. Zhang, S. Quan, X. Zhu, S. Shen, 3D numerical study of the liquid film distribution on the surface of a horizontal-tube falling-film evaporator, *Int. J. Heat Mass Transf.*, 124 (2018) 943–952.
- [32] Q. Qiu, X. Zhu, L. Mu, S. Shen, An investigation on the falling film thickness of sheet flow over a completely wetted horizontal round tube surface, *Desal. Wat. Treat.*, 57 (2016) 16277–16287.
- [33] M. Fiorentino, G. Starace, Numerical investigations on two-phase flow modes in evaporative condensers, *Appl. Therm. Eng.*, 94 (2016) 777–785.
- [34] A. Baloch, H. Ali, F. Tahir, Transient Analysis of Air Bubble Rise in Stagnant Water Column Using CFD, ICTEA International Conference Thermal Engineering, 2018.
- [35] R. Gupta, D.F. Fletcher, B.S. Haynes, On the CFD modelling of Taylor flow in microchannels, *Chem. Eng. Sci.*, 64 (2009) 2941–2950.
- [36] R.J.G. Lopes, R.M. Quinta-Ferreira, Assessment of CFD-VOF method for trickle-bed reactor modeling in the catalytic wet oxidation of phenolic wastewaters, *Ind. Eng. Chem. Res.*, 49 (2010) 2638–2648.
- [37] T.H. Nigim, J.A. Eaton, CFD prediction of the flashing processes in a MSF desalination chamber, *Desalination*, 420 (2017) 258–272.
- [38] J. Brackbill, D. Kothe, C. Zemach, A continuum method for modeling surface tension, *J. Comput. Phys.*, 100 (1992) 335–354.
- [39] W.H. Lee, A Pressure Iteration Scheme for Two-Phase Modeling, Technical Report LA-UR 79-975, Los Alamos Scientific Laboratory, Los Alamos, New Mexico, 1979.
- [40] A. Inc., Ansys Fluent Theory Guide, in: 15.0, SAS IP, Inc., 2013, pp. 591–593.
- [41] E. Da Riva, D. Del Col, Numerical simulation of laminar liquid film condensation in a horizontal circular minichannel, *J. Heat Transf.*, 134 (2012) 051019.
- [42] W. Nusselt, Die oberflächenkondensation des wasserdampfes, *VDI-Zs*, 60 (1916) 541–546.
- [43] S.M. Hosseinnia, M. Naghazadegan, R. Kouhikamali, CFD simulation of water vapor absorption in laminar falling film solution of water-LiBr — drop and jet modes, *Appl. Therm. Eng.*, 115 (2017) 860–873.
- [44] H. Ding, P. Xie, D. Ingham, L. Ma, M. Pourkashanian, Flow behaviour of drop and jet modes of a laminar falling film on horizontal tubes, *Int. J. Heat Mass f.*, 124 (2018) 929–942.
- [45] C.Y. Zhao, W.T. Ji, P.H. Jin, Y.J. Zhong, W.Q. Tao, Hydrodynamic behaviors of the falling film flow on a horizontal tube and construction of new film thickness correlation, *Int. J. Heat Mass Transf.*, 119 (2018) 564–576.
- [46] A. Bakker, Applied Computational Fluid Dynamics, CFD Lect., (2006) 1–35. Available at: <http://www.bakker.org/>.
- [47] Y. Zhou, Z. Cai, Z. Ning, M. Bi, Numerical simulation of double-phase coupled heat transfer process of horizontal-tube falling film evaporation, *Appl. Therm. Eng.*, 118 (2017) 33–40.
- [48] M. Li, Y. Lu, S. Zhang, Y. Xiao, A numerical study of effects of counter-current gas flow rate on local hydrodynamic characteristics of falling films over horizontal tubes, *Desalination*, 383 (2016) 68–80.
- [49] F. Sun, S. Xu, Y. Gao, Numerical simulation of liquid falling film on horizontal circular tubes, *Front. Chem. Sci. Eng.*, 6 (2012) 322–328.
- [50] C. Qi, H. Feng, H. Lv, C. Miao, Numerical and experimental research on the heat transfer of seawater desalination with liquid film outside elliptical tube, *Int. J. Heat Mass Transf.*, 93 (2016) 207–216.
- [51] L. Yang, Y. Liu, Y. Yang, S. Shen, Microscopic mechanisms of heat transfer in horizontal-tube falling film evaporation, *Desalination*, 394 (2016) 64–71.
- [52] Q. Qiu, X. Zhu, L. Mu, S. Shen, Numerical study of falling film thickness over fully wetted horizontal round tube, *Int. J. Heat Mass Transf.*, 84 (2015) 893–897.
- [53] J.D. Killion, S. Garimella, Simulation of Pendant droplets and falling films in horizontal tube absorbers, *J. Heat Transf.*, 126 (2004) 1003.
- [54] V. Subramaniam, S. Garimella, From measurements of hydrodynamics to computation of species transport in falling films, *Int. J. Refrig.*, 32 (2009) 607–626.
- [55] V. Subramaniam, S. Garimella, Numerical study of heat and mass transfer in lithium bromide-water falling films and droplets, *Int. J. Refrig.*, 40 (2014) 211–226.
- [56] G. Ji, J. Wu, Y. Chen, G. Ji, Asymmetric distribution of falling film solution flowing on hydrophilic horizontal round tube, *Int. J. Refrig.*, 78 (2017) 83–92.
- [57] Z. Xie, D. Pavlidis, J.R. Percival, J.L.M.A. Gomes, C.C. Pain, O.K. Matar, Adaptive unstructured mesh modelling of multiphase flows, *Int. J. Multiph. Flow*, 67 (2014) 104–110.
- [58] J.J. Cooke, L.M. Armstrong, K.H. Luo, S. Gu, Adaptive mesh refinement of gas-liquid flow on an inclined plane, *Comput. Chem. Eng.*, 60 (2014) 297–306.
- [59] A.D.G.H. Jasak, Automatic resolution control for the finite-volume method, Part 2: adaptive mesh refinement and coarsening, *Numer. Heat Transf. Part B Fundam.*, 38 (2000) 257–271.
- [60] R. Abraham, A. Mani, Heat transfer characteristics in horizontal tube bundles for falling film evaporation in multi-effect desalination system, *Desalination*, 375 (2015) 129–137.
- [61] F. Wunder, S. Enders, R. Semiat, Numerical simulation of heat transfer in a horizontal falling film evaporator of multiple-effect distillation, *Desalination*, 401 (2017) 206–229.
- [62] J. Chen, R. Zhang, R. Niu, Numerical simulation of horizontal tube bundle falling film flow pattern transformation, *Renew. Energy*, 73 (2015) 62–68.
- [63] J.D. Killion, S. Garimella, Gravity-driven flow of liquid films and droplets in horizontal tube banks, *Int. J. Refrig.*, 26 (2003) 516–526.
- [64] R. Armbruster, J. Mitrovic, Heat Transfer in Falling Film on a Horizontal Tube, Proceedings of the National Heat Transfer Conference, Portland, 1995, pp. 13–21.
- [65] X. Zhang, C. Meng, Q. Qiu, S. Quan, S. Shen, A numerical investigation of liquid film flow and film thickness distribution outside a horizontal tube, *Int. J. Low-Carbon Technol.*, 13 (2018) 424–431.
- [66] Q. Qiu, C. Meng, S. Quan, W. Wang, 3-D simulation of flow behaviour and film distribution outside a horizontal tube, *Int. J. Heat Mass Transf.*, 107 (2017) 1028–1034.
- [67] H. Hou, Q. Bi, H. Ma, G. Wu, Distribution characteristics of falling film thickness around a horizontal tube, *Desalination*, 285 (2012) 393–398.
- [68] D. Gstoehl, J.F. Roques, P. Crisinel, J.R. Thome, Measurement of falling film thickness around a horizontal tube using a laser measurement technique, *Heat Transf. Eng.*, 25 (2004) 28–34.

- [69] X. Chen, S. Shen, Y. Wang, J. Chen, J. Zhang, Measurement on falling film thickness distribution around horizontal tube with laser-induced fluorescence technology, *Int. J. Heat Mass Transf.*, 89 (2015) 707–713.
- [70] I.A. Hassan, A. Sadikin, N.M. Isa, The Numerical Modelling of Falling Film Thickness Flow on Horizontal Tubes, AIP Conference Proceedings, Vol. 1837, 2017, p. 020020. doi: 10.1063/1.4981161.
- [71] A. Stärk, K. Loisel, K. Odier, A. Feßenbecker, A. Kempter, S. Nied, H. Glade, Wetting behaviour of different tube materials and its influence on scale formation in multiple-effect distillers, *Desal. Wat. Treat.*, 55 (2015) 2502–2514.
- [72] P. Fernandez de Arroiabe, A. Martinez-Urrutia, X. Peña, M. Martinez-Agirre, M.M. Bou-Ali, Influence of the contact angle on the wettability of horizontal-tube falling films in the droplet and jet flow modes, *Int. J. Refrig.*, 90 (2018) 12–21.
- [73] M. Fernandez de Arroiabe, P. Martinez Urrutia, A. Alonso, L. Martinez-Agirre, M. Bouali, CFD Simulation of the Influence of Contact Angle in Falling Film Heat Exchangers, in: 13ème Congrès Mécanique, 11–14 Avril, Meknès, MAROC, 2017.
- [74] S.A. Khan, F. Tahir, A.A.B. Baloch, M. Koc, Review of micro-nanoscale surface coatings application for sustaining dropwise condensation, *Coatings*, 9 (2019) 117.
- [75] L. Románszki, M. Mohos, J. Tlegdi, Z. Keresztes, L. Nyikos, A comparison of contact angle measurement results obtained on bare, treated, and coated alloy samples by both dynamic sessile drop and Wilhelmy method, *Period. Polytech. Chem. Eng.*, 58 (2014) 53–59.
- [76] D. Polster, H. Graaf, Advancing and receding angles – Dynamic contact angle measurements on mixed alkyl monolayers, *Appl. Surf. Sci.*, 265 (2013) 88–93.
- [77] J.D. Bernardin, I. Mudawar, C.B. Walsh, E.I. Franses, Contact angle temperature dependence for water droplets on practical aluminum surfaces, *Int. J. Heat Mass Transf.*, 40 (1997) 1017–1033.
- [78] X. Liu, Y. Zhao, S. Chen, S. Shen, X. Zhao, Numerical research on the dynamic characteristics of a droplet impacting a hydrophobic tube, *Phys. Fluids*, 29 (2017) 062105.
- [79] L. Xu, M. Ge, S. Wang, Y. Wang, Heat-transfer film coefficients of falling film horizontal tube evaporators, *Desalination*, 166 (2004) 223–230.
- [80] J.M. Gonzalez, G.J.M.S. Jabardo, W.F. Stoecker, Falling Film Ammonia Evaporators, 1992. Available at: <http://hdl.handle.net/2142/9734>.
- [81] A.A. Mabrouk, K. Bourouni, H.K. Abdulrahim, M. Darwish, A.O. Sharif, Impacts of tube bundle arrangement and feed flow pattern on the scale formation in large capacity MED desalination plants, *Desalination*, 357 (2015) 275–285.
- [82] W.-T. Ji, C.-Y. Zhao, D.-C. Zhang, S. Yoshioka, Y.-L. He, W.-Q. Tao, Effect of vapor flow on the falling film evaporation of R134a outside a horizontal tube bundle, *Int. J. Heat Mass Transf.*, 92 (2016) 1171–1181.
- [83] D. Yung, J.J. Lorenz, E.N. Ganić, Vapor/liquid interaction and entrainment in falling film evaporators, *J. Heat Transf.*, 102 (1980) 20.
- [84] C.-Y. Zhao, W.-T. Ji, P.-H. Jin, W.-Q. Tao, Cross vapor stream effect on falling film evaporation in horizontal tube bundle using R134a, *Heat Transf. Eng.*, 39 (2018) 724–737.
- [85] F. Tahir, A.A. Mabrouk, M. Koc, CFD analysis of spray nozzle arrangements for multi effect desalination evaporator, Proceedings of the 3rd Thermal and Fluids Engineering Conference, 2018, pp. 935–941.
- [86] X. Zeng, M.-C. Chyu, Z.H. Ayub, Experimental investigation on ammonia spray evaporator with triangular-pitch plain-tube bundle, Part II: evaporator performance, *Int. J. Heat Mass Transf.*, 44 (2001) 2081–2092.
- [87] A. Altaee, A. Mabrouk, K. Bourouni, P. Palenzuela, Forward osmosis pretreatment of seawater to thermal desalination: high temperature FO-MSF/MED hybrid system, *Desalination*, 339 (2014) 18–25.
- [88] M.W. Shahzad, K. Thu, Y. Kim, K.C. Ng, An experimental investigation on MEDAD hybrid desalination cycle, *Appl. Energy*, 148 (2015) 273–281.
- [89] M.W. Shahzad, K.C. Ng, An improved multievacaporator adsorption desalination cycle for Gulf Cooperation Council countries, *Energy Technol.*, 5 (2017) 1663–1669.
- [90] C.Y. Zhao, W.T. Ji, Y.L. He, Y.J. Zhong, W.Q. Tao, A comprehensive numerical study on the subcooled falling film heat transfer on a horizontal smooth tube, *Int. J. Heat Mass Transf.*, 119 (2018) 259–270.
- [91] M. Christians, J.R. Thome, Falling film evaporation on enhanced tubes, part 2: Prediction methods and visualization, *Int. J. Refrig.*, 35 (2012) 313–324.
- [92] M. Christians, J.R. Thome, Falling film evaporation on enhanced tubes, part 1: Experimental results for pool boiling, onset-of-dryout and falling film evaporation, *Int. J. Refrig.*, 35 (2012) 300–312.
- [93] L. Yang, W. Wang, The heat transfer performance of horizontal tube bundles in large falling film evaporators, *Int. J. Refrig.*, 34 (2011) 303–316.
- [94] W.H. Parken, L.S. Fletcher, V. Sernas, J.C. Han, Heat transfer through falling film evaporation and boiling on horizontal tubes, *J. Heat Transf.*, 112 (1990) 744.
- [95] I. Newson, Heat transfer characteristics of horizontal tube multiple effect (HTME) evaporators - possible enhanced tube profiles, Proceedings of 6th International Symposium on Fresh Water from the Sea, 1978, pp. 113–124.
- [96] V.N. Slesarenko, Thermal desalination of sea water in thin film-plants, *Desalination*, 45 (1983) 295–302.
- [97] L. Yang, S. Shen, Experimental study of falling film evaporation heat transfer outside horizontal tubes, *Desalination*, 220 (2008) 654–660.
- [98] L.S. Fletcher, V. Sernas, W.H. Parken, Evaporation Heat transfer coefficients for thin sea water films on horizontal tubes, *Ind. Eng. Chem. Process Des. Dev.*, 14 (1975) 411–416.
- [99] M.-C. Chyu, A.E. Bergles, An analytical and experimental study of falling-film evaporation on a horizontal tube, *J. Heat Transf.*, 109 (1987) 983.
- [100] J. Mitrovic, Preventing formation of dry patches in seawater falling film evaporators, *Desal. Wat. Treat.*, 29 (2011) 149–157.
- [101] P.H. Jin, C.Y. Zhao, W.Q. Tao, Numerical Simulation of Falling Film Cooling on a Horizontal Smooth Tube, 5th Asian Symposium on Computational Heat Transfer and Fluid Flow, Bosan, Korea, 2015.
- [102] R. Kouhikamali, S.M.A. Noori Rahim Abadi, M. Hassani, Numerical investigation of falling film evaporation of multi-effect desalination plant, *Appl. Therm. Eng.*, 70 (2014) 477–485.
- [103] S. Bigham, R. Kouhikamali, S.M.A. Noori Rahim Abadi, Two-phase flow numerical simulation and experimental verification of falling film evaporation on a horizontal tube bundle, *Desal. Wat. Treat.*, 55 (2015) 2009–2022.
- [104] A.E. Al-Rawajfeh, S. Ihm, H. Varshney, A.N. Mabrouk, Scale formation model for high top brine temperature multi-stage flash (MSF) desalination plants, *Desalination*, 350 (2014) 53–60.
- [105] L. Yang, C. Gu, Z. Xu, X. Zhang, S. Shen, Numerical analysis on flow and heat transfer of a tube bundle in a horizontal-tube falling film evaporator, *Desal. Wat. Treat.*, 55 (2015) 3336–3342.
- [106] R. Abraham, A. Mani, Effect of flame spray coating on falling film evaporation for multi effect distillation system, *Desal. Wat. Treat.*, 51 (2013) 822–829.
- [107] A.T. Conlisk, Analytical solutions for the heat and mass transfer in a falling film absorber, *Chem. Eng. Sci.*, 50 (1995) 651–660.
- [108] V.E. Nakoryakov, N.I. Grigor'eva, Heat and mass transfer in film absorption with varying liquid-phase volume, *Theor. Found. Chem. Eng.*, 29 (1995) 242–248.
- [109] S.M. Saboya, F.E. Saboya, Experiments on elliptic sections in one- and two-row arrangements of plate fin and tube heat exchangers, *Exp. Therm. Fluid Sci.*, 24 (2001) 67–75.
- [110] Q.L. Li, S.L. Li, X.W. Zhang, B.C. Liu, L.X. Ma, M. Pahl, Heat transfer characteristics and flow behaviors of elliptic cylinders in crossflow, *J. Qingdao Univ. Sci. Technol.*, 25 (2004) 434–440.
- [111] Q.L. Li, L.X. Ma, S.L. Qi, C. Zhong, M.H. Pahl, Experimental investigation on heat transfer and flow resistance of an 1.6/1.0

- elliptic cylinder in crossflow, *J. Qingdao Univ. Sci. Technol.*, 25 (2004) 54–61.
- [112] L.C. Luo, G.M. Zhang, J.H. Pan, M.C. Tian, Flow and heat transfer characteristics of falling water film on horizontal circular and non-circular cylinders, *J. Hydrodyn.*, 25 (2013) 404–414.
- [113] Y.J. Cheng, Y.H. Liao, C.K. Huang, Heat transfer on a radially rotating heated cylinder, *Int. Commun. Heat Mass Transf.*, 35 (2008) 1355–1359.
- [114] K. Khanafer, S.M. Aithal, Mixed convection heat transfer in a lid-driven cavity with a rotating circular cylinder, *Int. Commun. Heat Mass Transf.*, 86 (2017) 131–142.
- [115] S. Lin, Z. Zhang, X. Liu, K. Zhuang, X. Li, Numerical study of falling film flow on a horizontal rotating tube, *Int. J. Heat Mass Transf.*, 117 (2018) 465–473.
- [116] J.C. Chato, *Laminar Condensation Inside Horizontal and Inclined Tubes*, Massachusetts Institute of Technology, 1960.
- [117] L. Gong, S. Shen, H. Liu, X. Mu, X. Chen, Three-dimensional heat transfer coefficient distributions in a large horizontal-tube falling film evaporator, *Desalination*, 357 (2015) 104–116.
- [118] S. Azimibavil, A. Jafarian Dehkordi, Dynamic simulation of a multi-effect distillation (MED) process, *Desalination*, 392 (2016) 91–101.
- [119] H. Louahlia-Gualous, L. El Omari, Local heat transfer for the evaporation of a laminar falling liquid film on a cylinder: experimental, numerical, and inverse heat conduction analysis, *Numer. Heat Transf. Part A Appl.*, 50 (2006) 667–688.
- [120] T.M. Pääkkönen, M. Riihimäki, C.J. Simonson, E. Muurinen, R.L. Keiski, Crystallization fouling of  $\text{CaCO}_3$  – Analysis of experimental thermal resistance and its uncertainty, *Int. J. Heat Mass Transf.*, 55 (2012) 6927–6937.
- [121] C. hua Qi, X. Han, H. qing Lv, Y. lei Xing, K. xin Han, Experimental study of heat transfer and scale formation of spiral grooved tube in the falling film distilled desalination, *Int. J. Heat Mass Transf.*, 119 (2018) 654–664.
- [122] A.E. Al-Rawajfeh,  $\text{CaCO}_3$ - $\text{CO}_2$ - $\text{H}_2\text{O}$  system in falling film on a bank of horizontal tubes: model verification, *J. Ind. Eng. Chem.*, 16 (2010) 1050–1058.
- [123] T.M. Pääkkönen, U. Ojaniemi, T. Pättikangas, M. Manninen, E. Muurinen, R.L. Keiski, C.J. Simonson, CFD modelling of  $\text{CaCO}_3$  crystallization fouling on heat transfer surfaces, *Int. J. Heat Mass Transf.*, 97 (2016) 618–630.
- [124] J.K. Min, D.H. Choi, Analysis of the absorption process on a horizontal tube using Navier ± Stokes equations with surface-tension effects, *Int. J. Heat Mass Transf.*, 42 (1999) 4567–4578.
- [125] D. Ouldhadda, A. Il Idrissi, M. Asbik, Heat transfer in non-Newtonian falling liquid film on a horizontal circular cylinder, *Heat Mass Transf. Und Stoffuebertragung*, 38 (2002) 713–721.
- [126] N. Giannetti, A. Rocchetti, S. Yamaguchi, K. Saito, Heat and mass transfer coefficients of falling-film absorption on a partially wetted horizontal tube, *Int. J. Therm. Sci.*, 126 (2018) 56–66.
- [127] F. Babadi, B. Farhanieh, Characteristics of heat and mass transfer in vapor absorption of falling film flow on a horizontal tube, *Int. Commun. Heat Mass Transf.*, 32 (2005) 1253–1265.
- [128] C. Woo Park, S. Soo Kim, H. Churl Cho, Y. Tae Kang, Experimental correlation of falling film absorption heat transfer on micro-scale hatched tubes, *Int. J. Refrig.*, 26 (2003) 758–763.
- [129] L. Hoffmann, I. Greiter, A. Wagner, V. Weiss, G. Alefeld, Experimental investigation of heat transfer in a horizontal tube falling film absorber with aqueous solutions of LiBr with and without surfactants, *Int. J. Refrig.*, 19 (1996) 331–341.
- [130] Y. Chen, R. Cao, J. Wu, Z. Yi, G. Ji, Alternate heat and mass transfer absorption performances on staggered tube bundle with M-W corrugated mesh guider inserts, *Int. J. Refrig.*, 66 (2016) 10–20.
- [131] I. Kyung, K.E. Herold, Y.T. Kang, Model for absorption of water vapor into aqueous LiBr flowing over a horizontal smooth tube, *Int. J. Refrig.*, 30 (2007) 591–600.
- [132] X. Hu, A.M. Jacobi, *Flow Characteristics of Liquid Droplets and Jets Falling Between Horizontal Circular Tubes*, Experimental Heat Transfer Fluid Mechanics and Thermodynamics, Edizioni ETS, PISA, 1997, pp. 1295–1302.
- [133] X. Hu, A.M. Jacobi, Departure-site spacing for liquid droplets and jets falling between horizontal circular tubes, *Exp. Therm. Fluid Sci.*, 16 (1998) 322–331.
- [134] J.-F. Roques, J.R. Thome, Falling film transitions between droplet, column, and sheet flow modes on a vertical array of horizontal 19 FPI and 40 FPI low-finned tubes, *Heat Transf. Eng.*, 24 (2003) 40–45.
- [135] J.J. Lorenz, D. Yung, Film breakdown and bundle-depth effects in horizontal-tube, falling-film evaporators, *J. Heat Transf.*, 104 (1982) 569.
- [136] P.L. Spedding, Falling Film Flow, in: *A-to-Z Guide to Thermodynamics Heat and Mass Transfer and Fluids Engineering*, Begellhouse, n.d. doi:10.1615/AtoZ.f.falling\_film\_flow.
- [137] X. Wang, T. Huai, Y. Li, Numerical simulation research of horizontal single-tube falling film evaporation, *Procedia Eng.*, 205 (2017) 1500–1506.